

Contents

1	Introduction	1
2	General Concepts	5
2.1	Escape rate	5
2.2	Constructing the repeller	6
2.2.1	Horseshoe Construction	7
2.2.2	Ensemble method	8
2.2.3	Single trajectory (PIM triple) method	9
2.3	The natural invariant distribution	11
2.4	Characterization of the natural measure	12
3	One-dimensional maps	13
3.1	The natural distribution and its relation to the conditionally invariant measure	14
3.1.1	The conditionally invariant measure	16
3.1.2	Frobenius-Perron equation	17
3.2	Thermodynamic formalism for repellers	19
3.2.1	Statistical analogy - Thermodynamic potentials	19
3.2.2	Spectra of the natural measure as thermodynamic quantities*	21
3.3	Eigenvalue formalism*	22
3.4	Other measures on the repeller*	24
4	Two-dimensional maps	25
4.1	Crisis and beyond	26
4.1.1	Configuration in phase space	26
4.1.2	Critical exponent of chaotic transients	27
4.2	A building block of chaotic repellers - the baker's transformation	30
4.3	Thermodynamics*	33
4.3.1	General setup*	33
4.3.2	Information dimensions and metric entropy*	36
4.3.3	Dimensions of stable and unstable manifolds and the uncertainty exponent	37
4.3.4	Maps with constant Jacobians*	38
4.4	Organization around periodic orbits	38
4.4.1	Qualitative picture	38
4.4.2	Length scales vs cycle eigenvalues*	39
4.4.3	Zeta functions*	40

5 Applications	41
5.1 Period doubling attractor	41
5.2 Models of disordered systems	43
5.2.1 Random field Ising chain	44
5.3 Irregular scattering	46
6 Discussion	50
7 Acknowledgments	52

Transient Chaos

1 Introduction

Transient phenomena have always played an important role in various fields of Science. In the last two decades we also learned that chaotic processes are common ubiquitous in the realm of nonlinear systems. The question then arises: Can transients display chaotic behaviour?

At first glance one might think the question is meaningless since chaos is an asymptotic property which manifests itself only after a very long observation of the system. Characteristics, e.g. Lyapunov numbers, are defined only in the infinitely long time limit. These features seem to be incompatible with the possibility of defining chaotic transients.

A somewhat more detailed analysis, however, leads to an affirmative answer. First, let us note that in experimental situations one never has infinitely long time intervals. In fact, what is needed for experimental observation of chaos is a well defined *separation of time scales*. Let t_0 denote the internal characteristic time of the system. In continuous time problems t_0 can be the average turnover time of trajectories in phase space or, in nonautonomous systems, the reciprocal value of the driving frequency, while in discrete dynamics it can be the time step itself. Suppose, one observes chaotic looking signals of average lifetime τ . A necessary condition for these signals to be chaotic is that they last much longer than the internal characteristic time, i.e.

$$\tau \gg t_0 . \quad (1)$$

If this criterion holds, one can apply the concepts worked out in the theory of dynamical systems in order to decide whether the signals are chaotic or not. The difference between permanent and transient chaos lies in the actual value of τ . In case of permanent chaos τ is practically infinite while transient chaos is characterized by a *finite* average lifetime τ . As a matter of fact, one cannot exclude the possibility that well known chaotic systems like, e.g., the Hénon attractor, would turn out to be

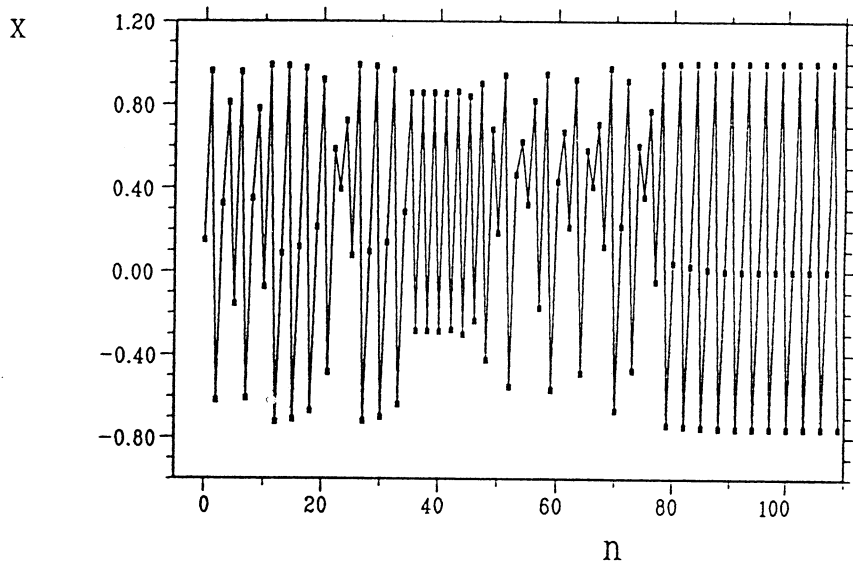


Figure 1: Transient chaotic signal of the logistic map $x_{n+1} = 1 - ax_n^2$ at parameter value $a = 1.75488$ where the attractor is a 3-cycle. This signal belongs to initial value $x_0 = 0.15$ and is chaotic up to 76 steps. The duration of the chaotic part is longer than the average lifetime which is $\tau = 31$ at this parameter value ($t_0 = 1$)

transiently chaotic during a much longer observation than usual. As for experiments, one follows a pragmatic view and requires for transient chaos τ to be of *human scales*, i.e. not to be longer than days.

A transiently chaotic signal has the following characteristic property. It looks chaotic up to length τ and then switches over, often quite abruptly, into a nonchaotic behaviour which governs all the rest of the signal. An example is shown in Figure 1.

It is an essentially new feature of transiently chaotic signals that by observing them in a phase space one finds, besides the actual attractor, another *invariant object* which is responsible for the irregular transients. These objects are called *chaotic* or *strange repellers*. In fact, in higher than one-dimensional systems they are often partially attractive, i.e. attractive along certain special hypersurfaces (stable manifolds) of the phase space and, therefore, they should be called *chaotic saddles*. In order to simplify the language we shall use here the term repeller also in higher dimensions. We mention in passing that strange repellers may, in principle, coexist with chaotic attractors. This corresponds to signals which exhibit a given type of chaotic behaviour on time scales τ and switch over into another type of chaos (having e.g. another Lyapunov exponent) asymptotically.

Note, transients of other type may also exist in dynamical systems. An example is provided by trajectories which approach an attractor but are far away from any repeller. These transients are nonpersistent and do not exhibit chaotic behavior although the true asymptotics might be chaotic. Thus, *transient to chaos* can be something completely *different* from transient chaos as the latter must be connected with an underlying strange repeller but the former not. In what follows we assume that the actual attractor is simple and study chaotic transients.

Trajectories starting from points of a chaotic repeller (or of its stable manifold) *never* leave the repeller and exhibit chaotic motion forever. It is, however, completely unlikely to hit such a point by random choice since the repeller is a set of *zero measure* (a *fractal*) and is globally not attractive. What is *observable* experimentally is not the repeller but rather a *small neighbourhood* of it. Trajectories starting close to the repeller can stay for a long time in its neighbourhood and show chaotic properties, but sooner or later they *escape* the neighbourhood. These are just the trajectories producing transiently chaotic signals. We shall also see that the *fractal* properties of chaotic repellers are *more* pronounced than those of attractors. Due to the interplay between chaos and escape, repellers are fractals along the *expanding* directions (unstable manifolds), too.

Another essential point in understanding transient chaos is the fact that one can define a *natural measure*, a special invariant distribution characterizing the motion on the repeller. Even more important is that an approximant to this distribution can be obtained experimentally. The approximate distribution is specified on a small neighbourhood of the repeller, just in the spirit of what has been discussed above. The advantage of having such a measure is that instead of temporal averages also *ensemble averages* can be taken just like for chaotic attractors. If one uses the approximate distribution, the averages will be subject to some errors the amount of which can always be estimated easily.

Historically, transient chaos was first observed in the Lorenz model for control parameter values (different from the standard one) where fixed points [1, 2] and a limit cycle [3] was the attractor. Subsequently, lots of theoretical papers [4]-[68] reported this phenomenon in all kinds of nonlinear systems: low-dimensional maps [8, 12], nonlinear oscillators [4, 14], delay equations [19], partial differential equations [24, 25] and coupled map lattices [35, 54]. The first comprehensive investigations were initiated by the discovery that chaotic transients appear typically in systems passing through a *crisis* configuration [16]. The importance of the natural measure on repellers and of quantities related to it were pointed out in Ref. [19] which gave new impetus to the research. More recent work deals with the characterization of the natural measure in which the application of the *thermodynamic formalism* turned out to be of great use [29, 41, 48].

The phenomenon of transient chaos is not at all restricted to physical systems. Biological time series are, e.g., good candidates for exhibiting this type of behaviour, a prototype of which could be data from epidemiology [69].

The first measurement in which chaotic transients were systematically observed was an experiment on Rayleigh-Bénard convection close to the critical Rayleigh number where transients were followed over days before settling down on a periodic attractor [70]. Afterwards a number of papers appeared reporting finite time chaotic behaviour in systems like: a compass forced by a magnetic field [71], a laser [72], the Rayleigh-Bénard convection at high Rayleigh numbers [73], electronic oscillators [74, 75], and a parametrically forced pendulum [76]. Nowadays a convection loop experiment [77] and a spin wave experiment [78] seem to provide the best represented

examples of measurements on chaotic transients. More recent investigations include also the dynamics of a bouncing ball [79], another laser system [80], a driven magnetoelastic ribbon [81] and the thermal convection in liquid crystals [82]. In spite of this impressive list, the experimental study of transient chaos seems to be much less extensive than the theoretical one. In many cases the phenomenon has only been mentioned and it is very well possible that transient chaotic signals have been considered to be uninterpretable and were therefore discarded. We hope this paper helps to fill in the gap between theory and experiment and encourages more quantitative measurements.

Finally, it is worth mentioning two further experimentally accessible phenomena strongly related to transient chaos. One is the appearance of *fractal basin boundaries* [16], [83]- [111]. If two or more attractors coexist in a system their basins of attraction are separated by basin boundaries. These boundaries might be fractals which has the consequence that trajectories started in their vicinity exhibit very complicated and unpredictable motion before settling down into one of the possible quite simple attractors. Basin boundaries are typically *stable manifolds* along which one or more *repellers*, situated between the attractors, can be approached [103]. In the case of fractal boundaries at least one of the repellers is *chaotic*. In fact, many observations of transient chaos, including also experiments (see eg. [72, 73, 74, 79, 80, 82, 89]) can be due to trajectories starting close to a fractal boundary separating multiple attractors.

Another phenomenon related to our subject is what is sometimes called *noise induced chaos*. First, let us notice that transients seem to be stable against noise [19]. In certain cases the increase of average lifetime τ has been observed in the presence of random perturbations [20]. It might also happen that noise pushes trajectories back in the vicinity of the deterministic repeller which leads then to an *asymptotic* chaotic behaviour (positive Lyapunov exponent along noisy trajectories) [89],[112]-[115]. This can be interpreted as noise induced chaos [113] the properties of which are strongly connected with that of the underlying deterministic repeller.

The aim of this paper is threefold. First, we would like to call the attention of experimentalists to the fact that a *quantitative* characterization of transient chaos is possible and that this can go beyond the measurement of the average lifetime to which all experiments have so far been restricted. Emphasis will be mainly on scaling or multifractal properties. Second, we summarize recent theoretical advances for low dimensional systems and show that they lead to a considerable increase in *accuracy*. Third, we present a few *applications*. We discuss briefly the case of *attractors* at the *onset* of chaos where these *universal* objects can be described via associated chaotic *repellers*. Furthermore, some models of *disordered systems* and the phenomenon of *irregular scattering* are presented to illustrate the use of these concepts beyond the scope of dissipative dynamical systems. (To assist readers not interested in theoretical aspects, technically more involved sections are marked by an asterisk (*).)

2 General Concepts

In this section we quantitatively characterize transient chaos. In order to have a consistent terminology, discrete time dynamical systems will be considered only. These can always be deduced from continuous time dynamics by taking an appropriately defined Poincaré map or a stroboscopic map, which roughly corresponds to taking repeatedly snapshots of the system at multiples of the characteristic time t_0 . By using such maps one reduces the dimensionality of the system by one and makes thus better visualization possible. In fact, Poincaré or stroboscopic maps have been obtained from experimental data on transient chaos and often proved to be low dimensional [75] - [81].

After observing chaotic looking signals on finite time scales one must answer the question if they are really chaotic. In the characterization of such signals we may distinguish different levels which can be summarized as

- measurement of the average lifetime, or escape rate,
- construction of the repeller in phase space,
- construction of the natural invariant distribution on the repeller,
- measurement of spectra characterizing the repeller and the distribution.

Following this hierarchy from top to bottom, one finds criteria for deciding whether the system is chaotic and, if so, also a measure for the strength of chaoticity. We discuss these levels separately.

2.1 Escape rate

In the Introduction we mentioned that typical trajectories escape any neighbourhood of the repeller. A quantity measuring how quickly this expulsion occurs is the so-called *escape rate* [17]. Let us imagine that a large number N_0 of initial points is distributed (uniformly) in a region Γ containing the repeller. Γ is supposed to be a simple set with a smooth boundary, e.g., a sphere. By iterating trajectories starting from the initial points, many will leave the region Γ after a certain number of steps. Let N_n denote the number of trajectories staying still inside Γ after n steps, and take N_0 so large that $N_n \gg 1$. As n gets large one observes, in general, an exponential decay in the number of survivors [2, 5, 8, 12, 13, 17, 18], that is, one finds asymptotically

$$\frac{N_n}{N_0} \sim \exp(-\kappa n) \quad (2)$$

where κ is the escape rate. A large κ value implies very strong repulsion. A vanishing escape rate means that the system loses its repelling property.

From a practical point of view the choice of region Γ is an important question. Theoretically, the asymptotic decay *does not* depend on the particular form of the

region, provided it does not contain the attractor. Therefore, one can simply take a finite phase space volume, cut out from it certain surrounding(s) of the attractor(s) and consider this as Γ . If one knows more or less where the repeller is situated, the best choice is a close neighbourhood, or a region with a large overlap, so as to avoid a very drastic decay in the number of survivors already in the first few steps. Anyhow, since the initial decay is not governed by the same law, general experience shows that one must wait up to a number of steps before trying to read off the escape rate from (2).

The definition of the escape rate tells us that the number of survivors decreases by a factor of $1/e$ after about $1/\kappa$ steps. This means that the majority of trajectories does not live longer than $1/\kappa$ in a region containing the repeller. Therefore, it is natural to identify this number with the average lifetime of transients, i.e. to write:

$$\tau = \frac{1}{\kappa}. \quad (3)$$

Note, this lifetime is the one with respect to a discrete dynamics. The lifetime in the corresponding continuous-time system is approximately given by t_0/κ . Note, this way of obtaining τ is more precise than a direct measurement from a time series since the end of a chaotic signal is not uniquely defined. An even more accurate method applies [18, 48, 66, 68] provided one succeeds in finding periodic orbits on the repeller (see section 4.4).

It is worth emphasizing that the existence of a well-defined positive lifetime for transients does not at all imply their chaoticity. One might also measure the effective Lyapunov exponents on time scales shorter than τ [3, 10, 40, 60] and find them to be positive. But notice, *trajectories around any kind of repeller have positive Lyapunov exponents* due to the repelling feature. In order to decide if the transients are really chaotic or not one needs more information. Qualitatively, the visual appearance (nonperiodicity) of the signal might help: around simple repellers trajectories should be regular. This is, however, only a hint, and more precise criteria require a direct study of the repeller's structure.

2.2 Constructing the repeller

We start the discussion with a numerical procedure illustrating the essence of chaotic repellers very clearly. Then we turn to a method which is well suited to analyze also experimental data since it is based on the investigation of ensembles of trajectories. Unfortunately, strange repellers have not yet been constructed in this (or any other) way from experiments. The construction is, however, feasible and, we believe, also unavoidable in order to find better contact between theory and experiment. Finally, a powerful numerical algorithm is presented.

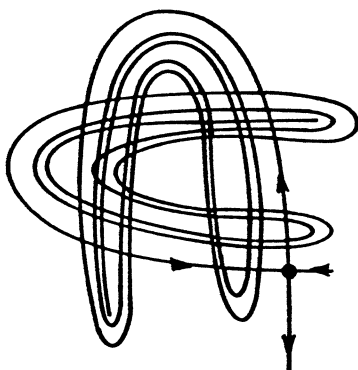


Figure 2: A horseshoe: schematic drawing of intersecting stable and unstable manifolds of a periodic orbit (fixed point) denoted by a dot

2.2.1 Horseshoe Construction

This method is based on the observation that unstable (hyperbolic) periodic orbits seem to cover a chaotic repeller densely, a property which is in common with chaotic attractors. Let us imagine that we choose a given hyperbolic periodic orbit in an *invertible* map and plot its stable and unstable manifolds, that is the surfaces along which the orbit is attractive in the direct and in the time-reversed motion, respectively. If these surfaces happen to cross each other once at so-called *homoclinic* points, they must do so infinitely many times since the images or preimages of such an intersection are again of the same type, forming together a homoclinic orbit. Homoclinic orbits never really reach the periodic orbit in question since they belong simultaneously both to its stable and unstable manifolds. Consequently, in such a situation the stable and unstable manifolds must have a complicated, intertwined structure. Figure 2 shows schematically how this can happen. The *horseshoe* [116] structure of the manifolds and the existence of homoclinic orbits have long been known as prerequisites for chaos [116, 117]. Interestingly, the stable and unstable manifolds of *different* periodic orbits of a strange repeller all run very close to each other and *all the homoclinic orbits belong to the chaotic repeller*.

Based on these observations, the following simple procedure is suggested for approximating a chaotic repeller in invertible maps. Find a hyperbolic orbit as simple as possible. This can be a fixed point or any short cycle. Plot its unstable and stable manifolds. The unstable manifold can be obtained by starting a large number of points in a small ball around the periodic orbit and iterating them forward. The stable manifold is obtained in an analogous way by using the inverted map. The intersections of these manifolds are parts of the repeller. Since only a finite number of branches of the manifolds can be constructed in practice, the intersections will provide us with an approximant to the repeller, which, however, can already reflect a *fractal* structure. Figure 3 displays stable and unstable manifolds in Hénon's map at parameter values where a strange repeller exists.

We thus accept as conditions for a repeller to be chaotic either the existence of

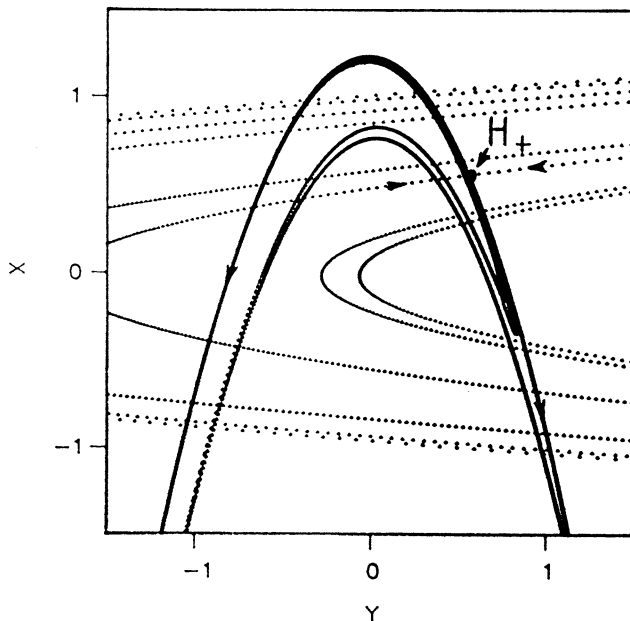


Figure 3: Stable and unstable manifolds of fixed point H_+ in the Hénon map $x' = 1 - ax^2 + by, y' = x$ at parameters $a = 2.0, b = 0.3$

a horseshoe in its manifolds, or a fractal geometry, along both stable and unstable directions of the repeller. (If the manifolds of the hyperbolic orbit we chose do not intersect each other, the orbit does not belong to a chaotic repeller.)

The procedure might be of use also in the problem of *fractal basin boundary*. In systems with inversion symmetry, e.g., the origin typically belongs to a repeller separating two or more attractors. By plotting the invariant manifolds of the origin, or any other hyperbolic periodic orbit, one can thus decide whether the orbit belongs to a chaotic repeller. If so, the stable manifold immediately provides us with the fractal basin boundary (or, in case of coexisting repellers, with a part of it).

It is worth emphasizing that for one-dimensional maps the horseshoe construction cannot be applied (the system is not invertible). Nevertheless, chaotic repellers are in such cases also fractals as will be illustrated in chapter 3.

Finally, we mention that the fractal structure of a repeller is equivalent to the statement that the *topological entropy* of the system is positive [119]. This means that the number of possible trajectories grows *exponentially* with the length. This has been known as the criterion for *weak chaos* [118] as it does not imply the positivity of the Lyapunov exponent on an *attractor*. It always implies, however, the existence of a horseshoe (the positivity of the Lyapunov exponent on the horseshoe is automatic). Therefore, it is a necessary and sufficient condition for transient chaos.

2.2.2 Ensemble method

The idea of this method, introduced in Ref.[19], is to follow an ensemble of trajectories and select the pieces of them which stay in the vicinity of the repeller. First one chooses arbitrarily a region around the expected position of the repeller, but

lying outside of the attractor. This can be the same region as Γ used in measuring the escape rate. Next, distribute a great number N_0 of initial points in this region uniformly, and iterate them forward. A criterion is needed for deciding when a trajectory is already far away from the repeller. The condition suggested in Ref.[19] was to study effective Lyapunov exponents over, say, 15 steps and ask if they were close to those characterizing the (nonchaotic) attractor. In case of fixed point attractors it was simply the negativity of all effective Lyapunov exponents which was interpreted as indication that the trajectory had left the repeller. All trajectories leaving the repeller earlier than n_0 steps are discarded. The choice of this number is somewhat arbitrary, it should grow with increasing lifetime τ . Experience shows, n_0/τ is a number not larger than 10. The idea is to select thus *long lived* trajectories in some broad surroundings of the repeller. Due to escape, of course, the majority of initial points drops out at this stage. If we liked to have about 10^3 trajectories of length not less than n_0 , the number N_0 of initial points is to be chosen as about $10^3 \exp(\kappa n_0)$ which can be in the order of 10^6 .

To select points really close to the repeller, these long lived trajectories are to be *truncated*. The first n_1 steps are to be discarded in order to forget initial conditions and to exclude points which happened to be close to the stable manifold but not yet to the repeller. The end of the long lived trajectories must be cut off, too, since the neighbourhood defined by the effective Lyapunov exponent method or by any other means need not be a close vicinity of the repeller. Therefore, in order to be sure that the points kept are really close to the repeller one discards the last $(n_0 - n_1)$ steps. Hence, only trajectories of minimal length n_0 give contribution.

The middle, truncated, parts of the long lived trajectories are then plotted in phase space and provide a good approximation of the repeller. An example is shown in Figure 4. It is to be checked, of course, if the result depends on the choice of N_0, n_0, n_1 , and if it does, one must try again with larger values until convergence sets in.

The method can, in certain cases, be somewhat simplified. First, instead of an extended region for initial points one may choose a straight line or a narrow strip in phase space. Second, we can avoid to follow effective Lyapunov exponents, which would be difficult experimentally, e.g. by finding in phase space a neighbourhood of the repeller. In fact, as escape takes place along unstable directions, one can generally select simple surfaces and say that trajectories are not yet far away from the repeller if they are still between these surfaces (for an example see the caption to Fig. 4).

2.2.3 Single trajectory (PIM triple) method

The aim of this method is to find a very long chaotic transient [52, 65] (see also [103]). The procedure is based on the fact that trajectories starting close to the stable manifold of the repeller stay for a long time in the vicinity of the repeller. The closer they start to the stable manifold the longer is their lifetime. For sake of simplicity

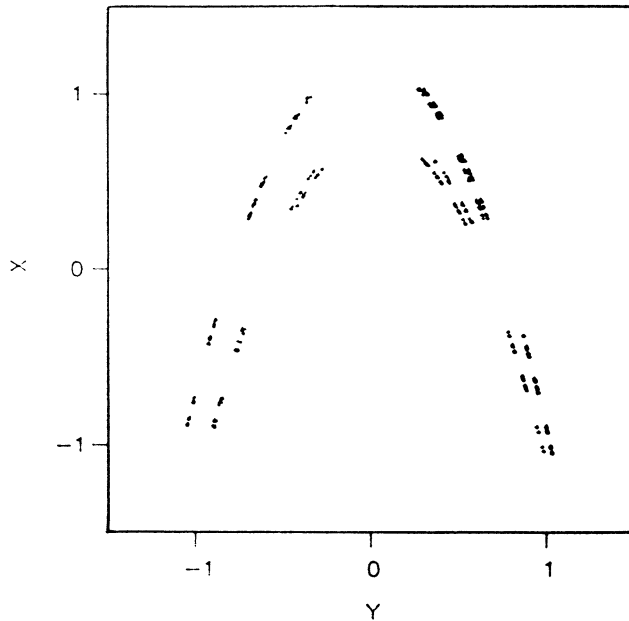


Figure 4: The repeller of the Hénon map at parameters $a = 2.0, b = 0.3$ obtained by the ensemble method. 10^6 initial points were distributed uniformly in the interval ($|y| < 0.5, x = 0$). Iteration was stopped for $|x| > 1.2$. The first 10 and the last 20 steps of long lived trajectories were discarded. Compare the repeller with the homoclinic points of Fig. 3

we give here the algorithm for systems with two-dimensional phase spaces. Take an interval \overline{AB} somewhere in the Poincaré plane so that it intersects the stable manifold of the repeller. Then choose initial points uniformly distributed on \overline{AB} and measure their lifetimes, i.e. the times until they exit a neighbourhood (e.g. Γ) of the repeller. Take then the point having the maximal lifetime inside the interval (i.e., the proper interior maximum - PIM). Its two neighbours are expected to lie on two different sides of a branch of the stable manifold. The two neighbours define a new interval $\overline{A'B'}$ on which the procedure can be repeated since the new interval will probably also intersect the stable manifold [65]. It is thus possible to continue the refinement of the original interval further in this way until the distance between neighbouring points is not smaller than some predetermined value $\delta \ll 1$. Take now the endpoints A'', B'' of the interval, on this finest level, containing the maximal lifetime point and iterate them forward. They approach the repeller along the stable direction but simultaneously move apart in the unstable direction. When the distance between these trajectories increases another predetermined value $\delta' > \delta$, stop iteration and refine the actual distance between the two trajectories, as described above, until a new interval shorter than δ is found.

By a subsequent repetition of iteration and refinement one then finds a series of intervals which are always within a tube of size δ' around branches of the stable manifold and, after a transitional time, also within a distance δ' of the repeller. Therefore, plotting any point of the intervals, after the transitional time, we find a

good approximant to the repeller.

In cases where the ensemble and PIM triple methods can be applied simultaneously, they yield identical results. The same repeller shown in Fig. 4 has been constructed in [52, 65] by means of the PIM triple algorithm. In general, one can say that the ensemble method is better suited for studying the repeller in systems with long average lifetime, whereas the PIM procedure can be applied also in cases where long transients are rather exceptional. The advantage of the latter is that the amount of error is well controlled, it would be, however, difficult to apply this procedure in experimental situations.

2.3 The natural invariant distribution

The natural invariant distribution $\mu(x)$ tells us how often different pieces of the repeller are visited by trajectories never escaping it [19]. (Such a natural measure exists also for nonchaotic repellers, but due to their simple geometrical structure, it has no special relevance, in contrast to chaotic cases.) Since neither infinitely long trajectories nor the precise fractal form of strange repellers are known, one is forced to work with an approximate natural measure. For this purpose, choose a fine but finite *coverage* of the repeller by *uniform boxes*, (cubes) of size $\epsilon \ll 1$. Next, consider points of trajectories which stay in a close vicinity of the repeller obtained, e.g., by the ensemble method. Let N denote the number of such nearby points, take all boxes which contain at least one nearby point and enumerate them. These nonempty boxes define a *coarse grained* repeller.

The approximate natural measure on a coarse grained repeller is given by the frequency showing how often different boxes are visited by truncated trajectories. More precisely, the approximate measure $P_i(\epsilon)$ of nonempty box i is [19]

$$P_i(\epsilon) = \frac{N_i}{N} \quad (4)$$

where N_i is the number of nearby points falling into box i . It is desirable to take N large enough so that $N_i \gg 1$ in nearly all nonempty boxes. $P_i(\epsilon)$ then provides a good approximation to the natural measure inside box i :

$$P_i(\epsilon) \simeq \int_{x \in \text{box } i} d\mu(x).$$

An example for an approximate natural distribution on a coarse grained repeller is given in Fig. 6. We emphasize, the procedure is applicable also to experimental data with a good statistics, provided the repeller has been constructed.

Points of asymptotic PIM triple trajectories (with an uncertainty $\delta' < \epsilon$) are expected to yield the same distribution $P_i(\epsilon)$.

It is worth mentioning that there exists also another strongly related measure the so-called *conditionally invariant* one [5], which is defined not on the repeller but rather on its unstable manifold, and can be used to construct the natural measure as will be illustrated in sections 3 and 4.

2.4 Characterization of the natural measure

Both the repeller and its natural invariant distribution might have complicated structures. Therefore, it is worth working out characteristics (which are simple numbers or simple functions of certain variables) even if they do not contain all the information the distribution does. These characteristics will be the analogues of those used in studying permanent chaos [120]-[137]. (We note that the characteristics can be worked out for *any kind of invariant distributions* but we give here the definitions with respect to the natural measure only. The generalization is straightforward.)

Let us consider first the *Lyapunov exponent*. For simplicity we assume that there is only one expanding direction in the system. Take a small interval of length Δ_0 along the unstable direction in a nonempty box i . It will be mapped after n steps on a longer interval of some length Δ_n . The *dilatation factor* Δ_n/Δ_0 can always be written as $\exp(\Lambda_{1i}(n))$ where the positive quantity $\Lambda_{1i}(n)$ is the *dilatation exponent* [122] belonging to box i . The Lyapunov exponent λ times n is simply the average of the dilatation exponent with respect to the (approximate) natural measure, i.e.

$$\lambda \simeq \frac{1}{n} \sum_i \Lambda_{1i}(n) P_i(\epsilon). \quad (5)$$

We repeat, the positivity of the Lyapunov exponent is not decisive for transient chaos as it characterizes all kinds of repellers.

Introduce, therefore, the set of *generalized* Lyapunov exponents λ_q [120]-[124] by studying the averages of the quantities $\exp(\Lambda_{1i}(n)q)$ where q is any real number. The generalized Lyapunov exponents can be obtained, for large values of n , from the relation [120, 122]

$$\sum_i e^{\Lambda_{1i}(n)q} P_i(\epsilon) \sim e^{q\lambda_q n}. \quad (6)$$

By taking the derivative for $q \rightarrow 0$ the Lyapunov exponent is recovered: $\lambda_0 = \lambda$. If the spectrum of Lyapunov exponents is found to be nontrivial, i.e. if $\lambda_q \neq \lambda_0$ for $q \neq 0$, the invariant object is necessarily a chaotic repeller.

The *fractal* properties of the repeller and the natural measure describe how quantities scale when changing the box size ϵ . According to standard definitions [125]-[134] the generalized dimensions D_q follow from the scaling form

$$\sum_i P_i(\epsilon)^q \sim \epsilon^{(q-1)D_q} \quad (7)$$

for decreasing ϵ . Chaotic repellers have, in general, nontrivial fractal properties.

Typically, one can associate a few symbols to different regions containing the repeller, and order a corresponding symbol to a trajectory step if it visits the given region. Thus, a *symbolic classification* [136] of trajectories around the repeller becomes possible. By following trajectories of length n around the repeller one can specify how often a given symbol sequence $\{S_j\}$ occurs. These path probabilities $P(\{S_j\})$ provide a complementary *dynamical* characterization of the system from

which the set of *generalized entropies* [135]-[137] can be deduced. The entropies K_q are defined for large n via the relation

$$\sum_{\{S_j\}} P(\{S_j\})^q \sim e^{(1-q)K_q n} \quad (8)$$

where the summation is taken over all occurring symbol sequences. K_0 is the topological entropy.

In summary, we give, in terms of the quantities introduced, a list of criteria from which the existence of a chaotic repeller and transient chaos follows:

- positivity of the topological entropy (implies in general the positivity of any other K_q), or
- noninteger fractal dimension D_0 or, in case of an integer D_0 , a nonconstant D_q distribution, or
- nontrivial λ_q spectrum.

As measures for chaoticity the topological entropy, the fractal dimension, or the Lyapunov exponent on the chaotic repeller can be used.

In hyperbolic cases, i.e. when the stable and unstable manifolds never touch each other tangentially (no homoclinic tangencies exist), the spectra λ_q , K_q and D_q are related in a simple way, as we shall see below.

In experimental analyses the dimensions would be best accessible as they can directly be deduced after measuring the box probabilities $P_i(\epsilon)$. The Lyapunov exponents and entropies are more difficult to obtain. If all periodic orbits of length n can be found (n not too large), they follow also from cycle properties [66] as will be discussed in section 4.4 (see also section 6). The topological entropy is, e.g., nothing but the logarithm of the number of n -cycles divided by n .

An application of the relations given above yields always results being subject to some errors due to finite resolution and statistics. How these errors can be minimized in low dimensional systems by using the thermodynamic formalism is the subject of the next sections.

3 One-dimensional maps

Strong dissipation causes drastic contraction in phase space which might lead to an approximately one-dimensional discrete map on a Poincaré plane. Such maps can, in fact, be found in experiments on transient chaos [75]. One-dimensional maps are typically *noninvertible* which distinguishes them from others arising from smooth flows. Therefore, one-dimensional maps are to be treated separately. They are not only simpler, but the investigation of them prepares the understanding of higher dimensional cases. As we shall see, what is going on in a one-dimensional

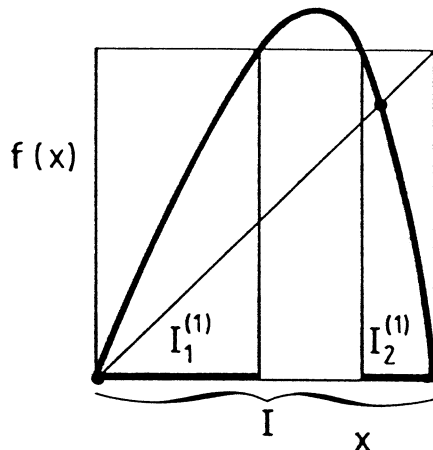


Figure 5: Typical map generating transient chaos on some interval I . Note that points lying outside the two subintervals $I_1^{(1)}$ and $I_2^{(1)}$ escape I after one time unit. Points which do not exit in n steps are contained in the $(n - 1)$ st preimages of the two subintervals (i.e. in the n th preimages of I), and exhibit chaotic behaviour, on time scale n , due to the global expansivity of the map

map generating transient chaos reflects exactly the behaviour along the *unstable* manifold of maps of the plane.

Transient chaos occurs if an interval I is mapped, under the dynamics $f(x)$, not into or onto itself but rather also partially *outside* itself. This implies, in general, a strong expansivity of the map. As an important class we shall consider here single humped functions, as illustrated in Figure 5. It is irrelevant how the map looks for x values outside I . In fact, there might be one or more attractors far away but if there is no feedback from these regions, the transient chaotic behaviour is completely specified by the function f defined *on* I .

In this chapter we study chaotic repellers and their invariant measures in maps belonging to the class defined by Fig. 5.

3.1 The natural distribution and its relation to the conditionally invariant measure

As mentioned earlier, chaotic repellers of one-dimensional maps can be constructed either by the ensemble method or by the PIM triple algorithm. Both procedures work well and can be used also for obtaining the approximate natural measure on a coarse grained repeller. As an illustrative example we use the map

$$x' = f(x) = 1 - ax^2 \quad (9)$$

which generates transient chaos for $a > 2$. The shortest interval I containing the repeller is then $(x^*, -x^*)$ where $x^* = -(1 + \sqrt{1 + 4a})/(2a)$ is the left fixed point of f . Figure 6 shows the approximate invariant measure on a repeller covered by uniform boxes of size $\epsilon = 2 \cdot 10^{-3}$.

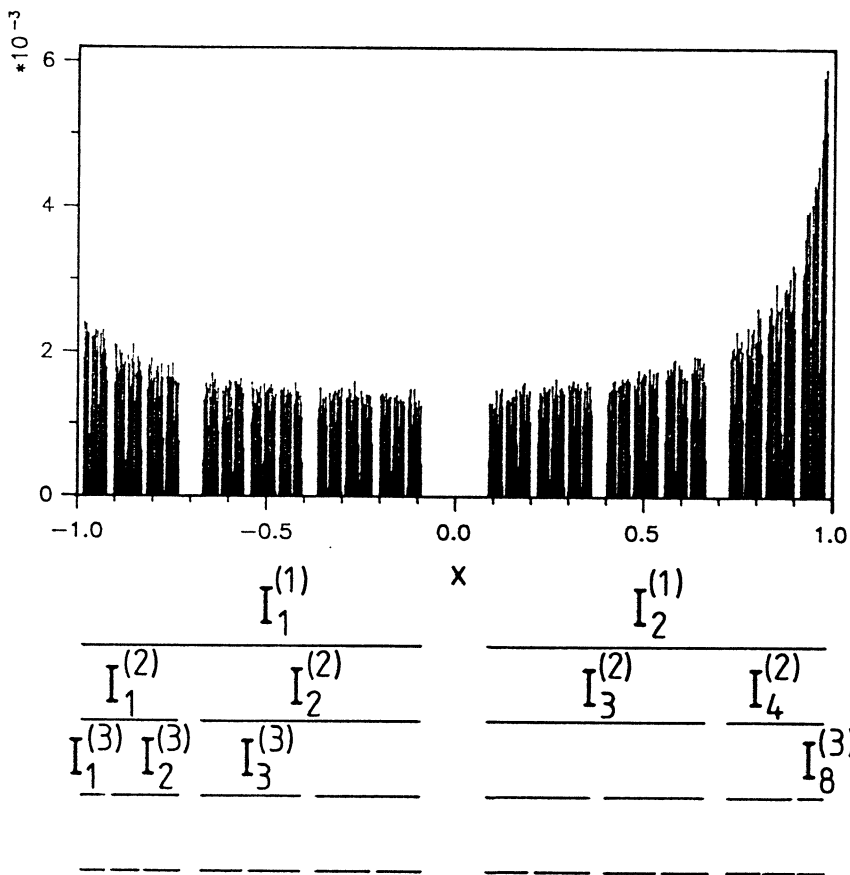


Figure 6: Natural distribution for map (9) at $a = 2.05$ obtained by the ensemble method on a grid of size $\epsilon = 0.002$. The number of initial points distributed uniformly in I was 10^7 , and the first 10 and the last 30 steps of trajectories were discarded. The truncated trajectories contained about 10^6 points ensuring a very good statistics. The escape rate was estimated by comparing the number of trajectories of length 10 and 30 in I which yields, via (2), $\kappa = 0.0711$. The lower part of the figure illustrates the organization of the repeller

Figure 6 contains also useful information concerning the repeller's structure. One easily notices that the crudest approximation to the repeller cover consists of two intervals, the two preimages $I_1^{(1)}$ and $I_2^{(1)}$ of I . At the next crudest stage each of them splits into two smaller intervals. By subsequent refinements a complete *hierarchy* is discovered, the n th level of which contains all the n th preimages of I . The preimage intervals are called *cylinders* and will be denoted by $I_i^{(n)}$. The subscript i enumerating them runs, at the n th level, up to 2^n . (Base 2 is a consequence of the double-valuedness of the inverse f^{-1} .) Note that the cylinders provide a coverage of the repeller with *nonuniform* boxes which, however, fits to the repeller's structure in a very natural manner. An equivalent way for defining the cylinders is to consider the n -fold iterated map f^n . Its graph is strongly oscillating and has 2^n branches (Fig. 7). The intervals which are mapped exactly onto I by the n -fold iterated map are just the cylinders of level n . This shows clearly that points in any $I_i^{(n)}$ do not

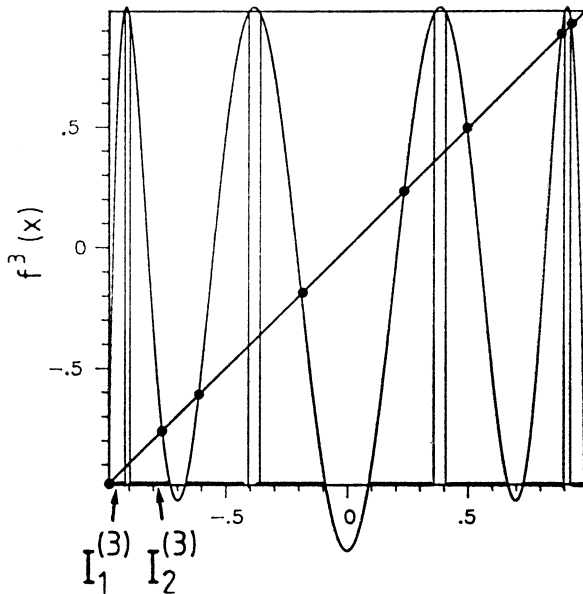


Figure 7: The threefold iterated map (9) at $a = 2.05$, and cylinders $I_i^{(3)}$. The dots denote 3-cycles

leave the basic interval I earlier than $n + 1$ steps. Notice, the folds with derivatives smaller than unity are, for sufficiently large n , always outside I . Thus, the maps investigated are *expansive* or, in other words, *hyperbolic* on the repeller.

3.1.1 The conditionally invariant measure

We now introduce the *conditionally invariant* measure [5] which is conceptually different from, but strongly related to, the natural one. The conditionally invariant measure (or *c-measure* for short) is defined on any region containing the repeller, and describes how trajectories escape this region. For simplicity, we take the latter to be I . Consider the conditional probability [5] that a given region is visited by trajectories (with random start in I) which do not escape I in m steps. Note, certain trajectories exit already in the next step. Their last points are, therefore, far away from the repeller and fill in the gaps between cylinders. Consequently, the conditional probability is defined on the *entire* interval I . The limit to which this conditional probability converges for $m \rightarrow \infty$ is the conditionally invariant measure.

The c-measure can be considered as one maintained by pumping new points into the system exactly according to the rate they escape it (formally, by multiplying the number of points everywhere by a constant in each step), so that an invariant distribution is obtained. The distribution tells us then how often certain regions are visited in the system which is subject to the afore-mentioned flux of points. Note, this formulation is general and applies also to higher dimensional systems.

It is easy to construct the conditional probability distribution for trajectories of minimal length m in the basic interval. One simply takes a modified version of the ensemble method in which the last steps are not discarded. Thus, only the first m

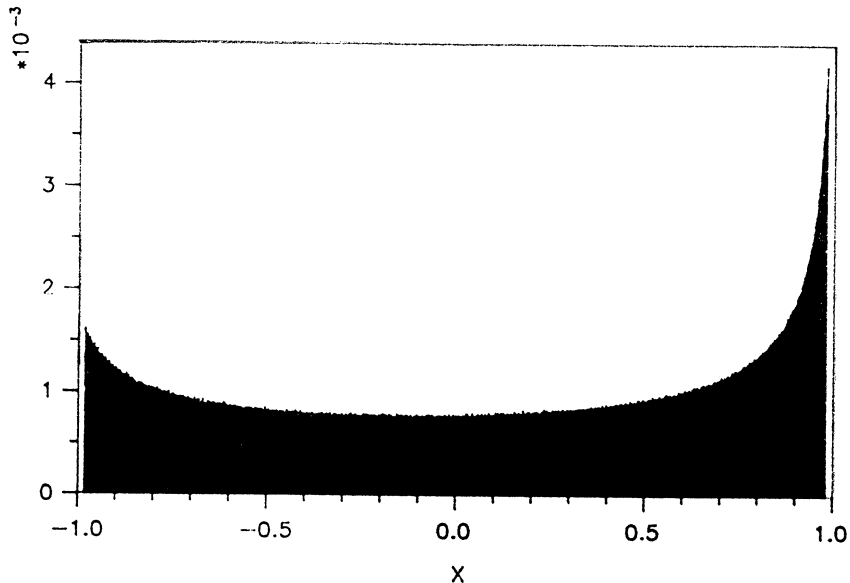


Figure 8: The conditionally invariant measure for map (9) obtained by discarding the first 10 steps of trajectories and plotting all points which stay inside the basic interval. Parameter, initial conditions and box size ϵ are the same as in Fig. 6.

steps are cut off and all the rest of trajectories is to be plotted before escaping I . Fortunately, the procedure converges exponentially fast and $m \sim 10$ provides already a very good approximation to the exact c-measure. Figure 8 shows the result for our illustrative example. Note, the measure has a *smooth density* everywhere in the basic interval.

To connect the conditionally invariant measure with the natural one let us *restrict* [19, 57] the density of the c-measure on cylinders of level n . This, of course, requires a renormalization so that the total measure on the cylinders is unity. The measures $\mu_i^{(n)}$ of intervals $I_i^{(n)}$ characterize then the motion of trajectories which end in one of the cylinders of level n . For n sufficiently large, these are the trajectories exhibiting long lived chaotic transients. Therefore, it is obvious that the limit of the cylinder measures $\mu_i^{(n)}$ obtained for $n \rightarrow \infty$ can be considered as the *exact* natural measure on the repeller [19].

We thus have two different approximants to the natural measure: the distribution P_i and that of $\mu_i^{(n)}$. The equivalence of the two methods can easily be illustrated. Figure 9 displays the c-measure restricted to cylinders of level 5. Alternatively, one can smooth out the approximate natural measure shown in Fig. 6 on the same set of cylinders. The resulting distribution is hard to distinguish from that of $\mu_i^{(n)}$ already at this relatively low level.

3.1.2 Frobenius-Perron equation

For a deeper understanding it is essential that the density $\varrho(x)$ of the conditionally invariant measure can be obtained also by *analytic* means. As shown in [5, 31] the

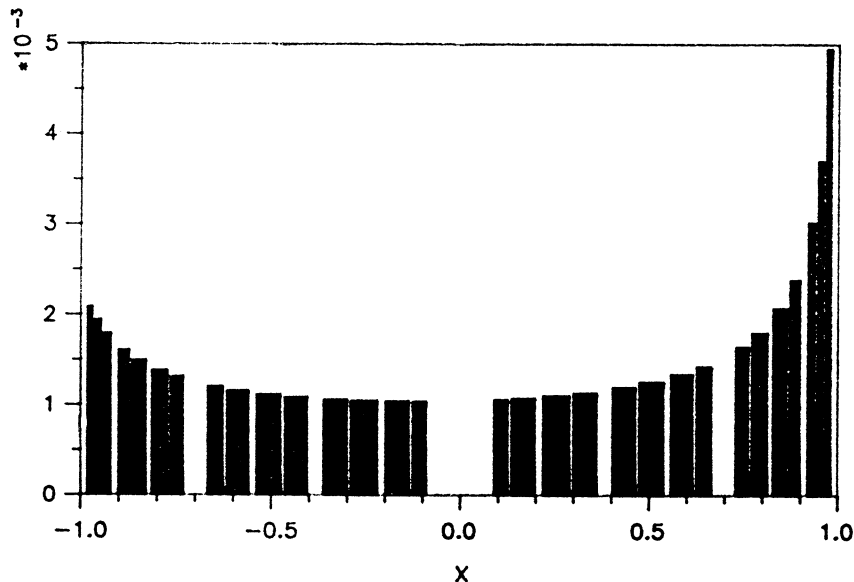


Figure 9: Measure obtained by restricting the conditionally invariant one of Fig. 8 to cylinders of level 5 specified by accuracy $\epsilon = 0.002$. (The two outmost cylinders are not resolved by the grid)

density follows from the iteration scheme

$$\varrho_n(x') = R \sum_{x \in f^{-1}(x')} \frac{\varrho_{n-1}(x)}{|f'(x)|} \quad (10)$$

where the summation is taken over the preimages of x' . By iterating any positive initial function $\varrho_0(x)$ on I the series $\varrho_n(x)$ will diverge or die out unless the coefficient R takes the value

$$R = e^\kappa. \quad (11)$$

With this R the series $\varrho_n(x)$ converges towards a finite limiting $\varrho(x)$ which is *independent* of the choice of the initial function, provided it is smooth. $\varrho(x)$ is the density of the c-measure. In practice, one tries different values for R until a convergence sets in. Fortunately, the convergence, if present, is rather fast and the limit can be reached with good accuracy at the 8th step [31] for the class of maps we are studying. An example is shown in Figure 10. One, thus, simultaneously finds both escape rate and density from an eigenvalue problem. In case of permanent chaos when $\kappa = 0$ (10) reduces to the well-known *Frobenius-Perron equation*.

By iterating (10) one clearly sees that a singularity builds up at the maximum of $f(x)$ but it is *outside* I . This supports again the view that the density of the conditionally invariant measure is a smooth function on neighbourhoods of hyperbolic repellers. Using the definition of the density, the cylinder measure $\mu_i^{(n)}$ can be expressed as

$$\mu_i^{(n)} = \frac{\int_{x \in I_i^{(n)}} \varrho(x) dx}{\sum_j \int_{x \in I_j^{(n)}} \varrho(x) dx}. \quad (12)$$

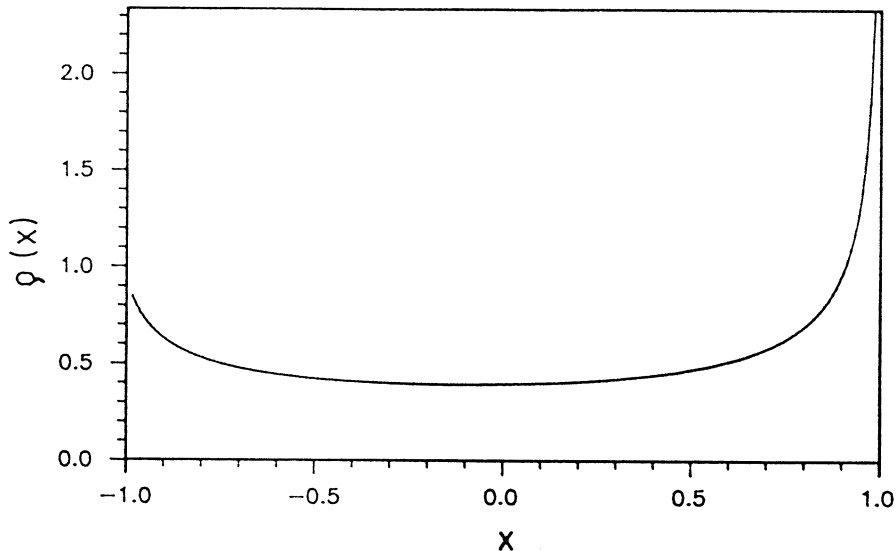


Figure 10: Density $\rho(x)$ of our illustrative example obtained from equation (10) as the 8th iterate of a constant initial function. (The relative error is 10^{-3})

This simplifies further if we take into account the fundamental observation concerning the smoothness of ρ which enables us to pull out the actual value of the density from the integrals, for sufficiently small cylinders. Since the density does not change with the refinement, the asymptotic scaling in n will be governed by the length scales alone. Thus one finds the simple statement that *the measure of a cylinder is proportional to its length*, more precisely

$$\mu_i^{(n)} \sim \frac{\epsilon_i^{(n)}}{\sum_j \epsilon_j^{(n)}} \quad (13)$$

where $\epsilon_i^{(n)}$ stands for the length of cylinder $I_i^{(n)}$. The n -independent proportionality factor not written out here depends on the actual form of ρ . This relation will play an essential role in what follows.

3.2 Thermodynamic formalism for repellers

3.2.1 Statistical analogy - Thermodynamic potentials

Based on classical mathematical papers [138] - [141], the thermodynamic formalism for chaotic systems has recently become a common tool also for physicists [142]-[156]. Here we show how the basic concepts work in one-dimensional maps with chaotic repellers.

Let us first notice that to each cylinder $I_i^{(n)}$ one can associate a unique symbol sequence $\{S_j\}$ ($j = 1, 2, \dots$) of length n . In single humped maps the symbols are binary and the convention can be used that S_j takes on the value 0 (1) if the

trajectory started in the cylinder is in step $j - 1$ left (right) from the maximum point, i.e., in the subinterval $I_1^{(1)}$ ($I_2^{(1)}$) (see Fig. 5). Consequently, the cylinders can be indexed also by the corresponding symbol sequences. Moreover, the cylinder measures are exactly the probabilities $P(\{S_j\})$ for finding a symbolic trajectory $\{S_j\}$ of length n :

$$\mu_i^{(n)} = P(\{S_j\}). \quad (14)$$

The key observation of the thermodynamical formalism is the unique connection between symbol sequences and *microstates of spin chains*. In fact, one can interpret symbol 0 (1) as a spin pointing down (up) and the whole string as a state of a spin chain of length n . In order to define the interaction between spins it turned out to be useful [138] - [141] to consider the logarithm of cylinder size to be proportional to the internal energy per spin in a given microstate:

$$E(\{S_j\}) = -\frac{1}{n} \log \epsilon_i^{(n)}. \quad (15)$$

Note, by this rule the additive constant of the energy scale has been fixed. The thermodynamic limit $n \rightarrow \infty$ corresponds to an ever refining coverage of the repeller. Eq.(15) reflects that the energies associated with cylinders stay finite when refining the partition.

In analogy with different multifractal spectra, one might wish to make a direct characterization of the length scale distribution of the cylinders by raising the length scales to a certain real power β and summing them all up at level n . The advantage of the statistical analogy just mentioned is that we now know, in view of (15), that $\epsilon_i^{(n)\beta}$ is a Boltzmann factor at temperature $1/\beta$. Their sum over all configurations is the partition function and, since the free energy is extensive, an exponential scaling is expected for large n :

$$\sum_i \epsilon_i^{(n)\beta} \sim e^{-\beta F(\beta)n}. \quad (16)$$

$F(\beta)$ is the free energy per spin and is called free energy also in the dynamical context ¹. The function $\beta F(\beta)$ is monotonically increasing with a negative second derivative (just like in thermodynamics), see Figure 11. The free energy and its Legendre transform with respect to β , the entropy $S(E) = \beta(E - F(\beta))$, provide a description of the length scale distribution and have been established as useful characteristics of general multifractals [29, 41], [143]-[156]. For practical purposes, the statistical analogy need not be worked out in more detail. What is essential for what follows is the scaling property (16) of length scale distributions generated by dynamical systems.

For our hyperbolic repellers the thermodynamic quantities are especially important since *all scaling* spectra defined in section 2 can be derived from them, owing to the relation between length scales and natural measures on cylinders.

¹In the mathematical literature $-\beta F(\beta)$ is called the topological pressure [138]-[141].

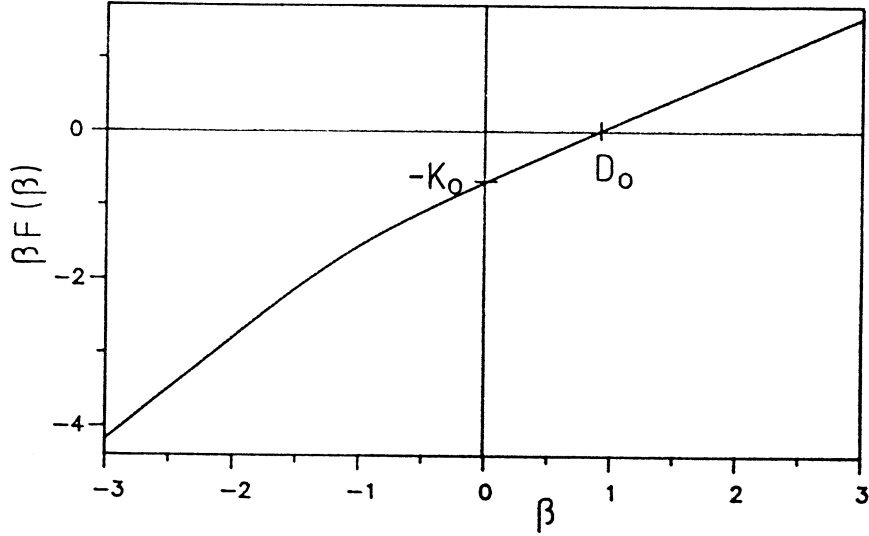


Figure 11: The free energy for map (9) at $a = 2.05$ in the range $|\beta| < 3$

3.2.2 Spectra of the natural measure as thermodynamic quantities*

First, notice that the total length of cylinders at level n is proportional to the number of points not yet escaped I after n steps. By recalling definition (2) we obtain

$$F(1) = \kappa. \quad (17)$$

The cylinder measures (13) can, therefore, be expressed as

$$\mu_i^{(n)} \sim e^{\kappa n} \epsilon_i^{(n)}. \quad (18)$$

To find the Lyapunov exponents, one observes that the logarithm of the slope of f^n at x is just the dilatation factor (c.f. section 2.4) in this point. The slope is, however, approximately constant in a cylinder as illustrated by Fig. 7. Since the length of I is of order unity, the dilatation factor in cylinder $I_i^{(n)}$ can be estimated as $1/\epsilon_i^{(n)}$. By comparing the definition of generalized Lyapunov exponents (6) with (16) and (18) we obtain

$$q\lambda_q = \kappa - (1 - q)F(1 - q). \quad (19)$$

The limit $q \rightarrow 0$ yields the usual Lyapunov exponent as

$$\lambda = \kappa + F'(1). \quad (20)$$

When calculating generalized dimensions, we use the famous relation [130, 132, 134]

$$\sum_k \frac{P_k^q}{l_k^{(q-1)D_q}} \sim 1 \quad (21)$$

where P_k and l_k denote measure and size of a box. Applying it to the cylinders and using (18), the left hand side will contain a sum involving the length scales $\epsilon_i^{(n)}$ which can be expressed by the free energy. We thus obtain an implicit relation

$$\beta F(\beta) \Big|_{\beta=q-(q-1)D_q} = \kappa q. \quad (22)$$

Interestingly, for the Legendre transform of the dimensions, i.e. for the $f(\alpha)$ [134] function of the natural measure, an explicit relation follows [29, 46]

$$f(\alpha) = \frac{S(E)}{E} \Big|_{E=\frac{\kappa}{1-\alpha}} \quad (23)$$

where $S(E)$ is the thermodynamic entropy.

Since the cylinder measures are simultaneously path probabilities (see eq.(14)), the generalized entropies can also be expressed by the free energy (use (8),(16) and (18)):

$$K_q = \frac{q(F(q) - \kappa)}{q - 1}. \quad (24)$$

By taking the limit $q \rightarrow 1$ in (22),(24) and by using (20), we obtain $K_1 = F'(1)$ and recover relations

$$K_1 = \lambda - \kappa = \lambda D_1, \quad (25)$$

first found in [19]. They tell us that for chaotic repellers the metric entropy K_1 is *not* identical with the Lyapunov exponent. Nevertheless, they are of equal sign since the information dimension D_1 is positive.

In summary, this is how to read off different characteristics after obtaining the graph $\beta F(\beta)$ vs. β :

- Escape rate: value at $\beta = 1$;
- Fractal dimension: intersection with the β axis;
- Topological entropy: the negative of the intersection with the vertical axis;
- Lyapunov exponent: slope at $\beta = 1$;
- Generalized dimension: subtracting κq yields intersection with the horizontal axis at $\beta = q - (q - 1)D_q$;
- Generalized entropies: subtracting $\kappa\beta$ yields $(\beta - 1)K_\beta$;
- Generalized Lyapunov exponents: subtracting κ yields $(\beta - 1)\lambda_{1-\beta}$.

3.3 Eigenvalue formalism*

The knowledge of the relations derived above has also practical relevance. A direct application of scaling forms (6)-(8) gives less precise results than those obtained through the thermodynamic formalism. The main reason is that we traced back everything to a coverage fitting naturally to the repeller and to length scales which are easy to measure. Even this accuracy can be improved by using an eigenvalue formalism.

Consider the recursion scheme [33]

$$Q_{n+1}(x') = R(\beta) \sum_{x \in f^{-1}(x')} \frac{Q_n(x)}{|f'(x)|^\beta} \quad (26)$$

which is an extension of (10) for real exponents β . Just like for $\beta = 1$, the iteration of any smooth positive function Q_0 on I leads to a finite limiting $Q^{(\beta)}$ with a special and unique choice of $R(\beta)$ only. We show now that this value must be

$$R(\beta) = e^{\beta F(\beta)}, \quad (27)$$

that is the complete free energy can be obtained as the leading eigenvalue of an operator (generalized Frobenius-Perron operator) defined by the right hand side of (26).

Take the n -fold iterated version of (26):

$$Q_n(x') = R(\beta)^n \sum_{x \in f^{-n}(x')} \frac{Q_0(x)}{|f^n'(x)|^\beta} \quad (28)$$

Assume we have the right $R(\beta)$ so that a finite limit exists. Since this limit is independent of the initial function we choose the latter to be identically 1. Thus, for sufficiently large values of n one finds

$$R(\beta)^{-n} = \frac{Z_n(\beta, x')}{Q^{(\beta)}(x')} \quad (29)$$

with

$$Z_n(\beta, x') = \sum_{x \in f^{-n}(x')} \frac{1}{|f^n'(x)|^\beta}. \quad (30)$$

Now we use again that inside cylinders the slope of the n -fold iterated function is approximately constant (see Fig. 7). The length of a cylinder containing point x can then be estimated as $1/|f^n'(x)|$, and Z_n is exactly the partition sum (16). Since the limiting function $Q^{(\beta)}$ is finite and independent of n , the left hand side of (29) must be $\exp(-\beta F(\beta)n)$.

Numerically, one evaluates Z_n for subsequent values of n and obtains the free energy from

$$\beta F(\beta) = \ln Z_{n-1}(\beta, x') - \ln Z_n(\beta, x') \quad (31)$$

where the x' -dependence disappears for large n . As an estimate for the error, the quantity $\ln(Z_n Z_{n-2}/Z_{n-1}^2)$ can be used. The convergence is again exponentially fast and, therefore, a few percent accuracy is obtained already at $n \sim 8$ for maps belonging to the class of Fig. 5. When going up to $n = 12$ the relative error is as good as 10^{-5} in a whole range $|\beta| < 10$. The free energy in Fig. 11 has been obtained by this method. If higher precision is needed one might use second and higher eigenvalues of the operator to find a more accurate fit for finite n [149, 62].

A special case of eq.(26) is the one obtained for $\beta = D_0$ [23]:

$$P_n(x') = \sum_{x \in f^{-1}(x')} \frac{P_{n-1}(x)}{|f'(x)|^{D_0}}. \quad (32)$$

This expresses that the iteration is compensated, no prefactor is needed, if the inverse temperature is just the fractal dimension of the repeller. In this sense, the equation can be considered as the Frobenius-Perron equation for repellers. In fact, the limiting distribution $P(x)$ provides a smooth covering curve for the natural distribution on the coarse grained repeller [23]. Eq.(32) provides a fast and accurate method for evaluating fractal dimensions of strange sets generated by one-dimensional maps. For our illustrative example it yields $D_0 = 0.905344$.

Another special form is

$$Q_{n+1}(x') = e^{\kappa q} \sum_{x \in f^{-1}(x')} \frac{Q_n(x)}{|f'(x)|^{q-(q-1)D_q}}. \quad (33)$$

This is a conversion of relation (22) into an eigenvalue equation and can be used to obtain the generalized dimensions (with respect to the natural measure) directly and with high accuracy from an iteration scheme [27, 38, 51].

3.4 Other measures on the repeller*

We briefly discuss other measures connected with repellers. A famous family is that of the so-called *Gibbs measures* [138] - [141],[29]. They are invariant under the map and are characterized by the property that the measure of a cylinder is proportional to a given *power of the length*. The exponent is the same for all cylinders and is a parameter of the measure. For order σ Gibbs measure the measure $\nu_i^{(n)}$ of cylinder $I_i^{(n)}$ is proportional to power σ of the length. With proper normalization this means that

$$\nu_i^{(n)} \sim \frac{\epsilon_i^{(n)\sigma}}{\sum_j \epsilon_j^{(n)\sigma}}. \quad (34)$$

The natural measure we discussed up to now is just the special case $\sigma = 1$. Since the measure is expressible through length scales, all spectra (6)-(8) for Gibbs measures can be given via the thermodynamic quantities $F(\beta)$ or $S(E)$. The relations are easy to derive along the lines of the previous section, here we just list them for the order σ Gibbs measure.

Lyapunov exponents:

$$q\lambda_q = \sigma F(\sigma) - (\sigma - q)F(\sigma - q). \quad (35)$$

Dimensions [33, 38, 39] :

$$\beta F(\beta) |_{\beta=\sigma q-(q-1)D_q} = \sigma F(\sigma)q. \quad (36)$$

The $f(\alpha)$ spectrum [147, 41] :

$$f(\alpha) = \frac{S(E)}{E} \Big|_{E=\frac{\sigma F(\sigma)}{\sigma-\alpha}} \quad (37)$$

Entropies [41] :

$$K_q = \frac{\sigma q (F(\sigma q) - F(\sigma))}{q - 1}. \quad (38)$$

Note that the Lyapunov exponent $\lambda = \lambda_0$ is just the derivative of $\beta F(\beta)$ taken at $\beta = \sigma$ [39] :

$$\lambda = \frac{d(\sigma F(\sigma))}{d\sigma}. \quad (39)$$

At $q = 1$ we find $K_1 = \sigma^2 F'(\sigma)$, and

$$K_1 = \sigma(\lambda - F(\sigma)) = \lambda D_1. \quad (40)$$

Since (26) holds, one can easily find also an equation yielding, e.g., D_q of the order σ Gibbs measure as an eigenvalue [38].

Another class of invariant measure on repellers is obtained by iterating the map *backward* in a *random* manner. By time reversal the repeller becomes an attractor and all random iterations approach this fractal set. Different distributions arise because of different ways of backward iteration. To each value x belong two preimages (if the map is single humped) denoted by $f_r^{-1}(x)$ where $r = 1$ if the preimage belongs to subinterval $I_1^{(1)}$, and $r = 2$ otherwise. The probability for taking branch 1 or 2 is to be decided. We suppose this depends on the actual position only and denote by $p_1(x)$ the probability for choosing branch 1. Obviously, $p_2(x) = 1 - p_1(x)$. The resulting distribution is a multifractal, the dimensions of which were shown [51] to be obtainable from the recursion scheme

$$Q_{n+1}(x) = \sum_{r=1}^2 \frac{Q_n(f_r^{-1}(x)) p_r^q(x)}{|f'(f_r^{-1}(x))|^{(1-q)D_q}} \quad (41)$$

as an eigenvalue, providing a powerful way for calculating this spectrum.

Nonnatural invariant measures play no central role in the dynamical context. They are worth studying, however, since in applications it might happen that a map generates a fractal as a repeller, but the distribution of physical relevance is not the natural one on the repeller but rather some of the above mentioned measures. Examples will be given in section 5.

4 Two-dimensional maps

Among higher dimensional systems we shall concentrate on invertible two-dimensional maps which are well suited for illustrating the most important new features. It is worth starting the discussion with a mechanism leading to the appearance of transient chaos and to the creation of strange repellers.

4.1 Crisis and beyond

4.1.1 Configuration in phase space

The phenomenon of boundary crisis [13] occurs if the basin boundary of a chaotic attractor touches the attractor itself. This is a marginal situation since certain points of the attractor belong simultaneously to the boundary (Figure 12). By changing parameters further, something drastic may occur: the boundary penetrates into the object having earlier been the attractor. This object is a union of unstable manifolds. The unstable manifold of any simple hyperbolic cycle, e.g. of a fixed point, has the shape of the strange attractor. If, however, the boundary cuts out pieces from the manifold, points on these pieces approach a neighbouring attractor lying somewhere beyond the boundary. In fact, if a piece is removed, so are all its preimages, which means that *nearly all points* of the unstable manifold are cut out (the origin of escape!), and the remnants form a fractal set, the repeller.

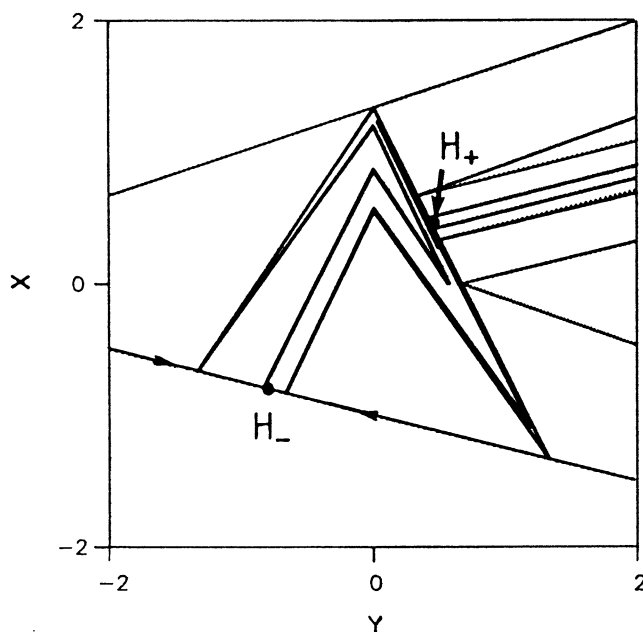


Figure 12: Invariant manifolds in the Lozi map: $x' = 1 - a |x| + by$, $y' = x$. The unstable manifold of the upper fixed point H_+ and the stable manifold of the lower one H_- (the basin boundary) are shown in a crisis configuration at $a = a_c = 1.75$, $b = 0.5$

This way of presenting a chaotic repeller is complementary to the horseshoe construction discussed in section 2. The basin boundary is a stable manifold, thus, what we generate now are *heteroclinic* points belonging simultaneously to stable and unstable manifolds of *different* hyperbolic objects. The resulting pictures are, however, equivalent since both homoclinic and heteroclinic points densely cover a chaotic repeller.

Figures 12 and 13 show a boundary crisis situation and a configuration where the

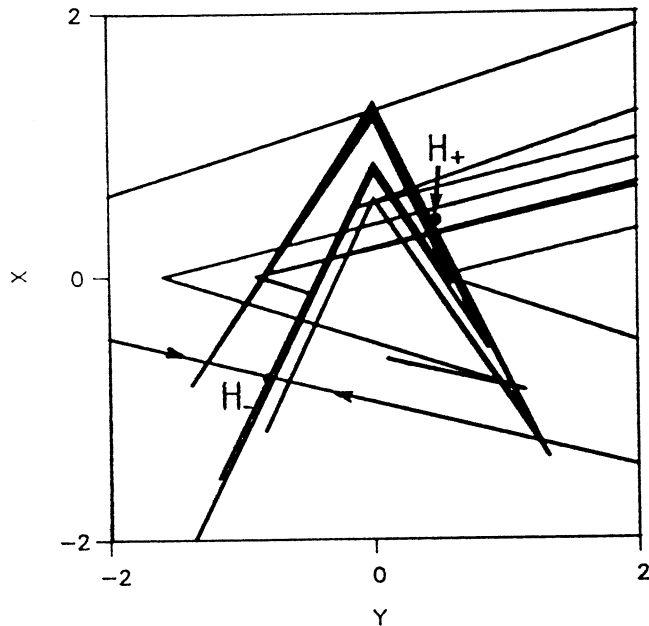


Figure 13: The same as Figure 12 but beyond crisis: $a = 1.8, b = 0.5$. The escaping feature is reflected also by the unboundedness of the unstable manifold. Local folds are cut out

chaotic attractor has been replaced by a strange repeller, respectively. A piecewise linear example has been chosen since all branches of stable and unstable manifolds can analytically be constructed in this case [157]. The topology of the manifolds is exactly the same as in the Hénon map. Figure 14 exhibits the repeller obtained via simulation what is to be compared with Fig.13.

Notice an essential property of repellers (Figs. 13,3): the local turning points of the unstable manifold are typically removed (just like the maximum of $f(x)$ in one-dimensional maps). These local folds are the places where homoclinic *tangencies* might occur, where local stable and unstable directions become degenerate. Such tangency points are, therefore, nonhyperbolic, the map is locally nonexpanding there. This observation explains why chaotic repellers are *often hyperbolic*, while strange attractors are probably generically nonhyperbolic. In what follows, therefore, we study the properties of hyperbolic chaotic repellers.

4.1.2 Critical exponent of chaotic transients

The escape rate just beyond crisis is generally small since tiny pieces of the unstable manifold are then cut out only. Therefore, such slightly supercritical configurations are the best candidates for *experimental* studies of transient chaos due to the persistence of long chaotic transients [75, 76, 78, 80, 81]. The escape rate has been shown [26, 34] to follow typically a power law behaviour as a nonlinearity parameter a passes through its crisis value a_c :

$$\kappa(a) \sim (a - a_c)^\gamma \quad (42)$$

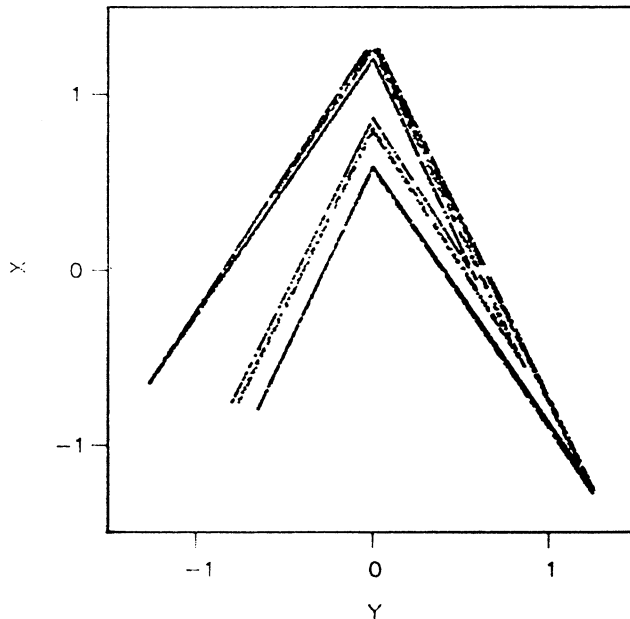


Figure 14: Repeller of the Lozi map at parameters $a = 1.8, b = 0.5$ obtained by applying the ensemble method. 10^4 trajectories were started along the interval $|y| < 0.8, x = 0$. Iteration was stopped if $|x|$ became larger than 1.3. The first 20 and the last 30 steps were discarded. A topologically similar repeller can be obtained in the Hénon map at $a = 1.5, b = 0.3$ which is just beyond a crisis configuration $a_c = 1.42692\dots, b = 0.3$

where γ is called the *critical exponent* of chaotic transients. This law has experimentally been verified in several cases [76, 78, 81].

A simple theoretical investigation shows [26, 34] that exponent γ depends essentially on the stability properties of a basic periodic orbit only.

Consider maps with *heteroclinic* tangency crisis, when the stable manifold of an unstable fixed point (H_- in Fig.12) is tangent to the unstable manifold of another hyperbolic fixed point (H_+) on the attractor. As a is increased slightly past a_c , the unstable manifold of H_+ crosses the stable manifold of H_- and the height of the overshoot away from both fixed points is proportional to $r \equiv a - a_c$ (Fig. 15). We suppose the local form of the unstable manifold in such tongues is a parabola of order z . ($z = 2$ is, of course, the generic case but for the Lozi map, e.g., $z = 1$ is relevant.) The width of the parabola piece lying outside the stable manifold is then of order $r^{1/z}$. Trajectories landed in this parabola piece (shaded region AB in Fig. 15) rapidly leave the repeller.

Take now the n th preimage of region AB . For n large enough, the deformation of the region is governed by the linearized map around H_+ . The n th preimage $A'B'$ has thus dimensions of the order of $r \exp(-\lambda_2^* n)$ and $r^{1/z} \exp(-\lambda_1^* n)$ where $\exp(\lambda_1^*)$ and $\exp(\lambda_2^*)$ denotes the modulus of the expanding and contracting eigenvalue at H_+ , respectively. Since after landing in $A'B'$ the trajectory soon (after n steps) falls

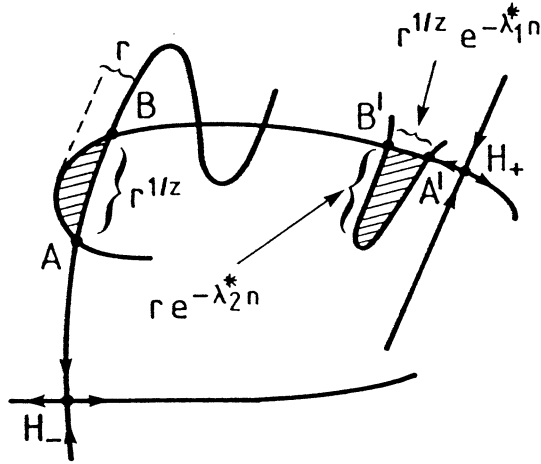


Figure 15: Schematic diagram illustrating the configuration of stable and unstable manifolds slightly beyond a homoclinic crisis

in AB , the escape rate can be estimated as the probability for landing in $A'B'$. The probability appearing here is the one associated with trajectories which are for a while in the vicinity of the repeller but then escape. Therefore, the *conditionally invariant measure* is to be used in this context. In leading order we can write

$$\kappa(a) \sim P_c(A'B') \sim r^\gamma \quad (43)$$

where $P_c(A'B')$ is the conditionally invariant measure of region $A'B'$.

The next step is to estimate how the conditionally invariant measure scales around fixed point H_+ . We use here an argument [56] which will be applied also later. As seen in one-dimensional maps, the conditionally invariant measure is *smooth* along the unstable direction. The new feature is that now a fractal structure is present in the unstable manifold when intersected along the stable direction. Consider a small box of size l_1 (l_2) along the local unstable (stable) direction. Its conditionally invariant measure scales, therefore, as

$$P_c(l_1, l_2) \sim l_1 l_2^{\alpha_2} \quad (44)$$

where $\alpha_2 < 1$ is a nontrivial exponent (crowding index) characterizing the local fractal structure.

Consider now a box containing fixed point H_+ . Its image has dimensions $l_1 \exp(\lambda_1^*)$, $l_2 \exp(\lambda_2^*)$ and lies around H_+ . Due to escape, the conditionally invariant measure of the original box and its image will be different. If, however, escape is compensated for by multiplying the original measure with $\exp \kappa$ (just like in one dimension) stationarity is found:

$$e^\kappa P_c(l_1, l_2) = P_c(l_1 e^{\lambda_1^*}, l_2 e^{\lambda_2^*}). \quad (45)$$

Using the scaling from (44) we immediately obtain

$$\lambda_1^* - \kappa + \lambda_2^* \alpha_2 = 0 \quad (46)$$

which connects the local crowding index with the eigenvalues at the fixed point.

As the scaling is the same everywhere around H_+ , we can apply (44),(46) to region $A'B'$. Close to crisis κ is small, therefore, in leading order $\alpha_2 = -\lambda_{1c}^*/\lambda_{2c}^*$ where the eigenvalues are taken *at* crisis. From (43) and (44) then

$$\gamma = \frac{1}{z} + \frac{\lambda_{1c}^*}{|\lambda_{2c}^*|} \quad (47)$$

follows (see [26, 34]). This is the desired relation telling us that the stability of H_+ at crisis and the topological properties of the map (z) completely specify the critical exponent.

In case of *homoclinic* tangency crisis when the stable and unstable manifolds of an unstable fixed point (or other periodic orbit) on the boundary are tangent (like, e.g., in Hénon type maps with positive Jacobian) a similar derivation yields [26, 34]

$$\gamma = \frac{1}{z} \frac{|\lambda_{2c}^*|}{|\lambda_{2c}^*| - \lambda_{1c}^*} \quad (48)$$

where the λ 's are now associated with the eigenvalues of the fixed point on the boundary, evaluated at crisis.

It has been pointed out [26, 34] that the eigenvalues of the basic periodic orbits can, in principle, be deduced in experiments. The first experimental determination of an unstable periodic orbit mediating crisis have been reported in [81].

For both type of crisis we have $\gamma > \gamma_0 = 1/z$ where γ_0 is the critical exponent for one-dimensional maps with local maxima of order z [75, 22, 31, 44]. This suggests that chaotic transients are *more persistent* in higher dimensional systems [34].

Finally, we note that the smoothness of the boundary has played an essential role in the derivation above. Crisis with a *fractal* basin boundary does not change the exponential decay (2) but may change scaling law (42). Transients in this cases can be very persistent so that the increase of κ can be slower than any power of $(a - a_c)$ [16, 20].

4.2 A building block of chaotic repellers - the baker's transformation

Locally, chaotic repellers seem to be the direct products of two Cantor sets. This can be best seen in the example of Figure 4. An elementary map producing a double fractal repeller is generated by the so-called baker's transformation. Its study may be useful also for experimentalists since it can probably be used as a first approximation in analyzing experimental data. In geometrical terms the action of such a transformation is the following: Take the unit square and cut it by a horizontal line into two pieces with surface area c and $1 - c$. The lower rectangle of width c is then stretched in the vertical direction by a factor $s > 1$ and simultaneously compressed in the horizontal direction by a factor $a < 1/2$ by keeping the left

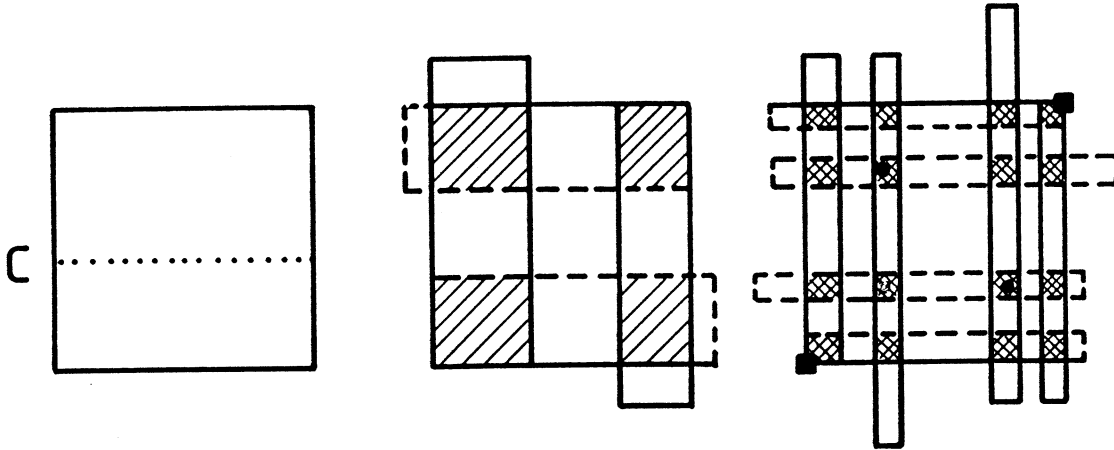


Figure 16: Images (continuous line) and preimages (dashed line) of the unit square under the baker's transformation. Points of the shaded and cross-shaded region do not escape the unit square after one and two steps, respectively, neither forward nor backward iterated. The black squares and the dots denote fixed points and a 2-cycle, respectively

lower corner fixed. The upper rectangle is to be transformed by a stretching and compressing factor $t > 1$ and $b < 1/2$, respectively, so that its right upper corner remains invariant. If stretching is sufficiently strong, i.e., $sc, t(1 - c) > 1$, the map generates transient chaos [23]. The analytic form of this transformation is

$$x' = ax, \quad y' = sy \tag{49}$$

for $y < c$, and

$$x' = 1 - b(1 - x), \quad y' = 1 - t(1 - y) \tag{50}$$

otherwise. The first two images of the unit square in forward and backward iteration are shown in Figure 16. (Notice that the inverted map is obtained by interchanging the role of x and y and by replacing s and t by $1/a$ and $1/b$, respectively. The constant c in the inverted map can be any number c' for which $c'/a, (1 - c')/b > 1$. The repeller's properties do not depend on the actual value of c and c' .)

Let us distribute N_0 initial points on the unit square uniformly. A portion c of them falls on the strip elongated by a factor s in the first step. Since only a ratio $1/sc$ of the total length overlaps with the unit square, the number of particles staying inside is just N_0/s . Analogously, from the other strip we find N_0/t survivors. Altogether, a portion of $1/s + 1/t$ of initial points does not escape the unit square in one time step. It is easy to check that this ratio stays constant as iteration goes on, therefore, the escape rate is $\kappa = -\ln(1/s + 1/t)$.

There is, of course, no stable limiting distribution of points on the unit square, due to escape. This can be compensated for by multiplying the number of particles staying *on* the unit square exactly by $\exp(\kappa)$ after each step. Thus, the number of points stays constant, and the probability of finding one of them in a certain region

defines a distribution. The probabilities of the two strips appearing in the first step are obviously $\exp(\kappa)/s$ and $\exp(\kappa)/t$. At the n th step there will be 2^n vertical strips of different widths. These widths can be expressed as $a^m b^{n-m}$, $m = 1, 2, \dots, n$. It is easy to check that the probability of finding particles in strip j of width $a^m b^{n-m}$ is just $\exp(\kappa n) s^{-m} t^{m-n}$. Notice that the term appearing behind $\exp(\kappa n)$ is just the reciprocal value of the dilatation factor $\exp(\Lambda_{1j}(n))$ for all points in a horizontal strip. Thus, we can express the conditionally invariant measure of strip j as

$$\mu_j^{(n)} = e^{\kappa n} e^{-\Lambda_{1j}(n)}. \quad (51)$$

Qualitatively, this means that unstable regions (large Λ_1) are less frequently visited. It is also clear that the limiting c-measure will be concentrated in infinitely narrow strips along unstable manifolds, and will have there a constant density.

Let us turn now to the natural measure. By overlapping the first preimage and image of the square, the common part contains points not escaping in the first step of the forward and backward iterations. Similarly, the union of the n th image and preimage defines trajectories staying inside the square at least n steps (Fig. 16) in both the direct and the inverted map. This clearly shows that never-escaping points belong to a double fractal, the repeller. Boxes generated by the overlap procedure provide a natural coverage (so-called generating partition [136]) to the repeller.

The width $\epsilon_{1i}^{(n)}$ of horizontal strip i is of type $s^{-m} t^{m-n}$, $m = 1, \dots, n$, i.e.

$$\epsilon_{1i}^{(n)} = e^{-\Lambda_{1i}(n)}. \quad (52)$$

Similarly, that of the vertical strips is

$$\epsilon_{2j}^{(n)} = e^{\Lambda_{2j}(n)}, \quad (53)$$

where Λ_{2j} is a contraction exponent (the dilatation exponent of the inverted map multiplied by (-1)). These sets are different, therefore the fractal properties along stable and unstable directions are also different. The proper way for characterizing such a direct product fractal is to introduce *partial* dimensions [131] $D_q^{(i)}$, $i = 1, 2$ ($i=1$ for the unstable direction) and to obtain the total dimensions by adding the partial ones.

In order to get the natural measure, the smooth density of the conditionally invariant one is to be restricted to boxes of the partition at level n , and is to be renormalized. Since the weight of a strip has been determined, the renormalization must be done by *keeping the measure of a strip constant*. This means that eq.(51) holds also for the natural measure of a strip. For the natural measure of a box of vertical size $\epsilon_{1i}^{(n)}$ inside a given vertical strip j one finds

$$\mu_{ij}^{(n)} = \mu_j^{(n)} e^{\kappa n} \epsilon_{1i}^{(n)} \quad (54)$$

The exact natural measure is then obtained in the $n \rightarrow \infty$ limit and the spectra of section 2 can easily be worked out.

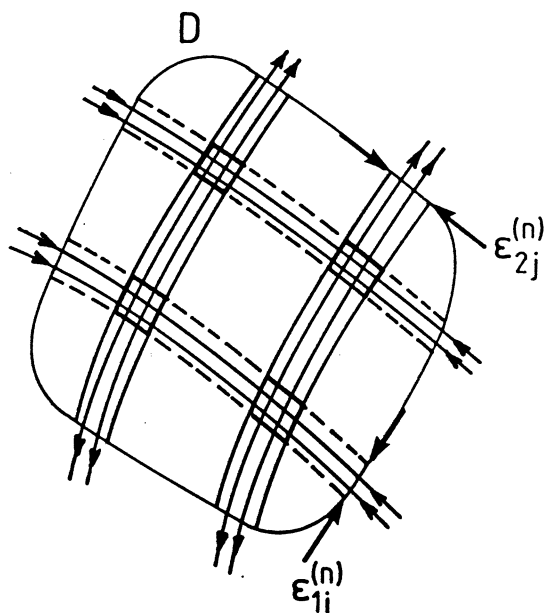


Figure 17: Schematic diagram of the phase space partition around a chaotic repeller obtained by taking the n th image and preimage of a region D . Stable strips (dashed lines), unstable strips (continuous lines) and invariant manifolds are shown. The boxes provide a coverage of the repeller

4.3 Thermodynamics*

4.3.1 General setup*

Let us consider now a general repeller. Take a region D of linear size of order unity containing the repeller, distribute many initial points on it and follow the iterates. The map stretches (compresses) D along the unstable (stable) direction and bends it so that a part of the image will lie outside D . After $n \gg 1$ iterations the overlap of the image with the original region will consist of narrow strips which follow locally the unstable direction of the repeller. We call them *unstable strips* (Fig. 17). As seen, the unstable manifolds behave smoothly around the repeller (folds are outside), therefore, unstable strips will only be slightly bent. The average width $\epsilon_2^{(n)}$ of an unstable strip is, by definition, proportional to the local contraction factors $\exp(\Lambda_2(n))$ of points falling, after n steps, in the strip. Due to escape, the majority of points will be outside the original region. If after each step the density of points inside D is multiplied just by $\exp(\kappa)$, a finite limit will be obtained. The resulting conditionally invariant measure has a *smooth* (but not necessarily constant) density along the unstable manifolds.

Without compensation, the measure of an unstable strip would be proportional to the area of its n th preimage. The preimage of D consists also of strips but these run parallel to the local stable directions of the repeller. The average width $\epsilon_1^{(n)}$ of such *stable strips* (Fig. 17) is proportional to the contraction factor of the inverted map, i.e. to $\exp(-\Lambda_1(n))$, where $\Lambda_1(n)$ is the dilatation exponent of points inside the strip. Consequently, the n th image of such a strip will have dimensions of order

unity and $\exp(\Lambda_2(n))$ along unstable and stable directions, respectively. We thus conclude that a stable strip is nothing but the n th preimage of an unstable one. The measure of an unstable strip without compensation would, therefore, be proportional to $\epsilon_1^{(n)}$. By taking into account also compensation, we find that the conditionally invariant measure in unstable strip j is

$$\mu_j^{(n)} \sim e^{\kappa n} \epsilon_{1j}^{(n)} \sim e^{\kappa n} e^{-\Lambda_{1j}(n)} \quad (55)$$

where $\epsilon_{1j}^{(n)}$ is the width of the n th preimage of unstable strip j .

The natural measure is obtained by taking the overlap between D 's n th image and preimage which defines a generating partition in the system and provides, for large n , a rather accurate coverage of the repeller. The natural measure of boxes in the partition follows then by redistributing the c-measure of unstable strips according to length scales $\epsilon_1^{(n)}$ inside the strips. Thus the natural measure of box i of length ϵ_{1i} lying in unstable strip j can be expressed as

$$\mu_{ij}^{(n)} \sim \mu_j^{(n)} e^{\kappa n} \epsilon_{1i}^{(n)}. \quad (56)$$

We emphasize again that $\mu_j^{(n)}$ as given by (55) is simultaneously the natural measure of strip j . Formally, this follows from $\sum \epsilon_{1i}^{(n)} \sim \exp(-\kappa n)$ which holds since escape takes place along the unstable direction only.

The natural measure of stable strips is also needed. By summing (56) over j one finds the natural measure of strip i as $\mu_i^{(n)} \sim \exp(\kappa n) \epsilon_{1i}^{(n)}$, the same as for its n th image. This reflects just the *preservation* of the natural measure under the map.

Qualitatively speaking, maps generating hyperbolic repellers can be locally decomposed into baker's transformations. Their actual form might change with the position but only smoothly. This is the reason why the general relations are similar to those obtained in the previous section.

In analogy to what has been done in one-dimensional maps, let us now define a free energy based on the length scales generated along the unstable direction:

$$\sum_i \epsilon_{1i}^{(n)\beta} \sim e^{-\beta F(\beta)n} \quad (57)$$

($F(1) = \kappa$). We show now that also Lyapunov exponents, partial dimensions $D_q^{(1)}$ and entropies can be derived from the free energy.

Note first that the dilatation factor for points of stable strip i is just $\exp(\Lambda_{1i}(n)) \sim 1/\epsilon_{1i}^{(n)}$. Next, observe that a given stable strip contains points having the same history (up to n steps at least), therefore, $\mu_i^{(n)}$ is simultaneously a path probability. Since the natural measure is proportional to length scales, relation (6),(8) can be expressed via the free energy, and eqs.(19) and (24) is easily recovered.

The partial dimensions along the unstable direction can be calculated via (21) with P_k as the natural measure inside *stable* strips and with length scales as the

widths of these strips:

$$\sum_i \frac{\mu_i^{(n)q}}{\epsilon_{1i}^{(n)(q-1)D_q^{(1)}}} \sim 1. \quad (58)$$

After expressing the measures with length scales one obtains

$$\beta F(\beta)_{|\beta=q-(q-1)D_q^{(1)}} = \kappa q. \quad (59)$$

For the Legendre transform $f_1(\alpha_1)$ of the partial dimensions this implies

$$f_1(\alpha_1) = \frac{S(E)}{E} \Big|_{E=\frac{\kappa}{1-\alpha_1}}. \quad (60)$$

Note, a comparison of (15) with the relation between length scales and dilatation exponent tells us that the energy of stable strip i is just

$$E = \frac{1}{n} \Lambda_{1i}(n). \quad (61)$$

Thus we see that for all properties connected with the unstable direction analog relations follow as in one-dimensional maps.

Quantities containing information also about the stable direction cannot be, in general, computed from the free energy. First one might think that another free energy should be introduced based on the length scales $\epsilon_{2j}^{(n)}$. This is, however, not sufficient since computing the partial dimension $D_q^{(2)}$ needs both widths $\epsilon_{2j}^{(n)}$ and measures $\mu_j^{(n)}$ of *unstable* strips. Therefore, it is worth defining a partition sum weighting length scales and measures differently. Let us write

$$\sum_j \mu_j^{(n)p} \epsilon_{2j}^{(n)\beta} \sim e^{-\beta G(\beta,p)n}. \quad (62)$$

Here p is a real parameter, the analog of pressure in thermodynamics. G is a bivariate function which can be called the Gibbs potential. In view of (55) the new partition sum is practically a sum over length scales arising along both stable and unstable directions in the generating partition. Note that β is different from that used in (57) and the free energy $F(p)$ is recovered at $\beta = 0$. The Gibbs potential provides in a sense the most general characterization of the repeller and its natural measure.

For $\beta = 0$ sum (62) contains the measures (path probabilities) only, consequently

$$\beta G(\beta, q)_{|\beta=0} = (1 - q)K_q. \quad (63)$$

By taking the limit $\beta \rightarrow 0$ at $p = 1$, the logarithm of eq.(62) yields just the averaged Lyapunov exponent $\lambda^{(2)} < 0$ in the stable direction:

$$\frac{\partial(\beta G(\beta, 1))}{\partial \beta} \Big|_{\beta=0} = -\lambda^{(2)}. \quad (64)$$

As another special case the partial dimensions $D_q^{(2)}$ follow from the condition

$$\beta G(\beta, q)|_{\beta=-(q-1)D_q^{(2)}} = 0 \quad (65)$$

which is equivalent to applying relation (21) in the form:

$$\sum_j \frac{\mu_j^{(n)q}}{\epsilon_{2i}^{(n)(q-1)D_q^{(2)}}} \sim 1. \quad (66)$$

The total D_q dimension is the sum of the partial ones [131, 122]. Eqs (63),(65) mean that the order q entropy and partial dimension along the stable direction can be read off as the intersection of the graph $\beta G(\beta, q)$ ($p = q$ fixed) with the vertical and the β axis, respectively. This shows also that the Gibbs potential contains much more information than entropies and partial dimensions (or the free energy) alone.

We note, the sets $\{\epsilon_1^{(n)}\}, \{\epsilon_2^{(n)}\}$ do *not* play equivalent roles in the formalism since the natural measure is connected with one of them only (cf.(56)). Consequently, by interchanging the subscripts 1,2 another measure, the natural distribution of the *inverted* map, will be characterized. With the exception of topological entropy and partial fractal dimensions these measure have nothing in common in dissipative cases.

Finally, a few consequences will be discussed.

4.3.2 Information dimensions and metric entropy*

Although eqs. (59),(65) are implicit, for the order 1 dimensions *explicit* expressions can be derived. A Taylor expansion of (65) around $q = 1$ and the application of (63),(64) leads to

$$K_1 = -\lambda^{(2)}D_1^{(2)}. \quad (67)$$

From the relations along the unstable direction

$$K_1 = \lambda D_1^{(1)} = \lambda - \kappa \quad (68)$$

follows. Thus, the information dimension along the unstable direction can be expressed as [19]

$$D_1^{(1)} = 1 - \frac{\kappa}{\lambda}, \quad (69)$$

that along the stable one as [42]

$$D_1^{(2)} = \frac{\lambda - \kappa}{|\lambda^{(2)}|}. \quad (70)$$

The total information dimension is their sum:

$$D^{(1)} = K_1 \left(\frac{1}{\lambda} + \frac{1}{|\lambda^{(2)}|} \right) \quad (71)$$

in harmony with the Kaplan-Yorke conjecture [127, 128].

4.3.3 Dimensions of stable and unstable manifolds and the uncertainty exponent

Stable and unstable manifolds of chaotic repellers seem to be the direct products of a Cantor set and a smooth curve (see Fig. 3). Consequently, their fractal dimensions appear as 1+ the dimension of a Cantor set. As the stable manifold intersects the unstable one just in points of the repeller, the points of intersection have the partial fractal dimension $D_0^{(2)}$ of the repeller. Thus, the dimension of the unstable manifold is [42]

$$d_U = 1 + D_0^{(2)}, \quad (72)$$

and similarly

$$d_S = 1 + D_0^{(1)} \quad (73)$$

for the stable one. The stable manifold is simultaneously a basin boundary, therefore, the fractal dimension of the boundary is $d_B = d_S$. Here we assume that the boundary is the stable manifold of a single repeller.

In case of fractal boundary, uncertainty in initial conditions leads to enhanced uncertainty in the final state. To characterize this property an exponent α has been introduced [83]. Cover the phase space (or a part of it) by boxes of linear size ϵ and count the number $N_u(\epsilon)$ of boxes from which initial conditions can asymptote to several attractors. The fraction of phase space with uncertain final state is expressed as $f = N_u(\epsilon)/N(\epsilon)$ where $N(\epsilon)$ is the number of boxes needed to cover the whole region of interest. This fraction is expected to scale with the initial uncertainty ϵ as

$$f \sim \epsilon^\alpha \quad (74)$$

where α is the *uncertainty exponent* [83]. Since boxes with uncertain final state cover the boundary, $N_u \sim \epsilon^{-d_B}$. As $N(\epsilon)$ changes like ϵ^{-2} ,

$$\alpha = 2 - d_B, \quad (75)$$

follows: exponent α is the codimension of the basin boundary. Eqs.(74),(75) provide a useful method for measuring d_B via the uncertainty exponent [83]-[111]. In view of the fact that the boundary is the stable manifold, eqs.(73),(75) imply

$$\alpha = 1 - D_0^{(1)} \quad (76)$$

demonstrating that the uncertainty exponent can be expressed via a characteristic of the *repeller*.

An upper bound to α can be given as $1 - D_1^{(1)}$. Thus, from (69) we obtain

$$\alpha \leq \frac{\kappa}{\lambda} = \frac{F(1)}{F(1) + F'(1)} \quad (77)$$

where the left hand side might actually be quite close to the exact value. For fixed point repellers and simple boundaries $\alpha = 1$.

4.3.4 Maps with constant Jacobians*

There is an important class of maps the Gibbs potential of which can be expressed by the free energy. These are maps with constant Jacobians. Constant Jacobian means that the area contracting ratio is position independent. Consequently, the product of the dilatation and contraction factors is spatially constant, i.e.

$$\Lambda_1(n, x) + \Lambda_2(n, x) = n \ln J \quad (78)$$

where J is the Jacobian. The width of an unstable strip j and its n th preimage are therefore related as $\epsilon_{2j}^{(n)} = J^n \epsilon_{1j}^{(n)}$ and the Gibbs potential takes the form:

$$\beta G(\beta, p) = (p + \beta)F(p + \beta) - \kappa p - \ln J \beta. \quad (79)$$

Condition (65) can then be rewritten as

$$\beta(F(\beta) - \ln J)_{|\beta=q-(q-1)D_q^{(2)}} = (\kappa - \ln J)q \quad (80)$$

which implies for the Legendre transforms

$$f_2(\alpha_2) = \frac{S(E)}{E - \ln J} \Big|_{E=(\kappa - \alpha_2 \ln J)/(1 - \alpha_2)}. \quad (81)$$

Thus, we conclude that in maps with constant Jacobians all scaling and fractal properties of the chaotic repeller and its natural measure can be deduced from the free energy alone. This is manifested also in the fact that relations exist among partial dimensions and entropies [56] which easily follow from (80,81).

4.4 Organization around periodic orbits

4.4.1 Qualitative picture

A direct determination of the length scales in a generating partition is not always easy. Therefore, a complementary approach is of great use which is based on hyperbolic *cycles* obtainable, in principle, also from time series of experimental data [158]. The basic idea is that periodic orbits densely cover strange sets. Consequently, chaotic motion can be interpreted as a *random walk among cycles*. This means that chaotic trajectories happen to behave as periodic with a given periodicity for a short time, but then they switch over to other temporary periodic behaviours again and again. They cannot follow a cycle forever since periodic orbits in chaotic systems are unstable. (In the transient chaotic signal of Fig. 1 ,e.g., a definite period-2 behaviour can be observed for about 12 time units.) If chaotic trajectories visit unstable cycles, the characteristics of chaotic motion must be expressible through cycle properties. From dynamical point of view the most relevant ones are stability (better instability) properties described by eigenvalues of the linearized n -fold iterated map in periodic orbits of length n (cycle eigenvalues for short). Thus, one expects that chaos can be

characterized by means of the cycle eigenvalues, provided sufficiently many periodic orbits can be analyzed. This programme has been worked out in detail [18], [158]-[164], including also transient chaos [18, 48, 55, 56, 66, 163, 68]. An advantage of this approach is the fact that, using the so-called zeta function [140, 48, 66, 68], very accurate results can be obtained already from rather short cycles. Here we summarize the main points of the method.

Notice first that cylinder lengths in one-dimensional maps can be expressed by cycle eigenvalues. The fixed points of the n -fold iterated map are just period- n points. They are obtained as the intersections of the diagonal with the graph of f^n . One sees immediately (Fig. 7) that each cylinder of level n contains one n -cycle. Since they belong to cylinders, the slopes of f^n at a cycle point is approximately the same as in any point of the cylinder containing this periodic orbit (a property used several times in section 3). Consequently, we find $\epsilon_i^{(n)} \sim 1/|f^n'(x_i^*)|$ where x_i^* is the n -cycle belonging to cylinder i . Thus, one can also say that it is the stability of periodic orbits what determines the partition function and the free energy.

4.4.2 Length scales vs cycle eigenvalues*

Consider now two-dimensional maps. Take an unstable strip and its n th preimage. The common part of them defines points which return approximately to their initial positions after n steps and must, therefore, contain an n -cycle. Let us write the moduli of the cycle eigenvalues as $\exp(\lambda_i(n))$, $i = 1(2)$ for the expanding (contracting) eigenvalues. The contracting eigenvalue of the period- n point in unstable strip j will define the width of this strip, i.e.

$$\epsilon_{2j}^{(n)} \sim e^{\lambda_{2j}(n)}. \quad (82)$$

Similarly, the width of the n th preimage strip is just the reciprocal value of $\exp(\lambda_{1j}(n))$:

$$\epsilon_{1j}^{(n)} \sim e^{-\lambda_{1j}(n)}. \quad (83)$$

Thus, one can express all relevant length scales and, in view of (55), (56), also the measures of strips via stability properties of the n -cycles. Consequently, we can write

$$\sum_i e^{-\lambda_{1i}(n)\beta} \sim e^{-\beta F(\beta)n} \quad (84)$$

and

$$\sum_j e^{-\lambda_{1j}(n)p} e^{\lambda_{2j}(n)\beta} \sim e^{-(\beta G(\beta,p) + \kappa p)n}. \quad (85)$$

It is instructive to see an equivalent local approach, too. Consider a box of dimensions l_1 and l_2 along unstable and stable directions, respectively, which contains an n -cycle point. For the c -measure of this box scaling form (44) holds. Applying the same argument which led in case of a fixed point to relation (46), we now find

$$\lambda_{1i}(n) - \kappa n + \lambda_{2i}(n)\alpha_2 = 0 \quad (86)$$

where α_2 is a local crowding index along the stable direction around the n -cycle point i . The natural measure inside the same box scales as

$$P(l_1, l_2) \sim l_1^{\alpha_1} l_2^{\alpha_2} \quad (87)$$

with $\alpha_1 < 1$ as the crowding index along the unstable direction. Owing to the relation between natural and conditionally invariant measures α_2 is in common for these measures. From the preservation of the natural measure an additional relation is obtained:

$$\lambda_{1i}(n)\alpha_1 + \lambda_{2i}(n)\alpha_2 = 0 \quad (88)$$

(which is formally the same as for chaotic attractors [160]). Equations (86),(88) show that the set of crowding indices can uniquely be determined by measuring the cycle eigenvalues. Based on the fact that $\lambda_{1i}(n)/n$ plays the role of the energy (see (61)), relations (60) and (81) can directly be derived from this local approach.

4.4.3 Zeta functions*

Note that the sums (84),(85) contain *all* n -cycles which are allowed to exist in the system. This means that the fixed point, e.g., appears also as an n -cycle. In general, certain cycles are repetitions of shorter ones. All are here included, not only the so-called *primitive* cycles which cannot be decomposed into more elementary ones.

The zeta function approach [140, 48, 66, 68] allows us to concentrate on primitive cycles only. Consider the free energy. Eq.(84) can be rewritten as

$$\sum_i z^n e^{-\lambda_{1i}(n)\beta} \sim 1, \quad (89)$$

with the condition that the smallest z value which makes the sum compensated (neither decay nor divergence) is just $z(\beta) = \exp(\beta F(\beta))$. Take now the expression

$$\Omega(z) = \sum_n \sum_i z^n e^{-\lambda_{1i}(n)\beta} \quad (90)$$

which, according to (89), must diverge at $z = z(\beta)$. Next, we use a basic property of periodic orbits: the eigenvalue is the same everywhere along such an orbit. Furthermore, each period n can be written as r repetitions of a primitive cycle of length n_p : $n = r n_p$. (For primitive cycles $r = 1$). Consequently, we have for all points i belonging to an n -cycle $\lambda_{1i}(n) = r \lambda_{1p}(n_p)$ where $\lambda_{1p}(n_p)$ is the dilatation exponent along a primitive cycle. Thus, the terms on the right hand side can be rearranged as a sum over all primitive cycles and a sum over repetitions

$$\Omega(z) = \sum_p n_p \sum_{r=1}^{\infty} (z^{n_p} e^{-\lambda_{1p}(n_p)\beta})^r. \quad (91)$$

The geometric sum can be summed up yielding

$$\Omega(z) = \sum_p \frac{n_p z^{n_p} e^{-\lambda_{1p}(n_p)\beta}}{1 - z^{n_p} e^{-\lambda_{1p}(n_p)\beta}}. \quad (92)$$

This can be written as z times the logarithmic derivative of the zeta function

$$\zeta_{\beta}(z) = \prod_p (1 - z^{n_p} e^{-\lambda_{1p}(n_p)\beta}). \quad (93)$$

Since a divergence in $\Omega(z)$ corresponds to a zero of $\zeta(z)$, the free energy follows from the *smallest positive root* of the zeta function.

An analogous argument based on (85) leads to the form

$$\zeta_{\beta,q}(z) = \prod_p (1 - z^{n_p} e^{-\lambda_{1p}(n_p)q + \lambda_{2p}(n_p)\beta}) \quad (94)$$

the smallest root of which yields $z(\beta, q) = \exp(\beta G(\beta, q) + \kappa q)$. For more general expressions see [68].

The advantage of the approach is that the zeta function was obtained after a *partial summation* over arbitrarily long trajectories. It is, therefore, not surprising that accurate results can be obtained by keeping only a few short primitive cycles in the products of (93),(94). An efficient computational tool, the *cycle expansion* [48, 66] is based on the fact that longer orbits can be approximately pieced together from a few short *fundamental* primitive cycles. The product in the zeta function can always be written as a sum over the fundamental cycles plus corrections. The latter contain differences of contributions from primitive cycles and from pseudo orbits pieced together from shorter primitive cycles and the fundamental ones. Since the pseudo orbits are typically close to real ones, the corrections are rather small and the cycle expansion converges exponentially fast. The method has successfully been applied for calculating escape rates, topological entropies and partial fractal dimensions of repellers [48, 66, 68] from cycle eigenvalues up to length $n \sim 6 - 12$.

5 Applications

5.1 Period doubling attractor

The onset of chaos is quantitatively identical for broad classes of systems. Theoretically, this *universal* behaviour is understood by applying a renormalization group transformation [165] which shows that many details are irrelevant and the relevant features can be described in terms of universal *one-dimensional* maps even if the original system is higher dimensional.

A typical route to chaos is the period doubling cascade. At the accumulation point of this cascade systems reach the borderline to chaos and possess an attractor, the so-called period doubling attractor, which is already much more complicated than a periodic one but is not yet really chaotic. The properties of this attractor can be understood by means of a one-dimensional map $x' = g(x)$ where g is a universal function, the fixed point of the afore-mentioned renormalization transformation [165]. The attractor is a fractal with a natural measure generated by a 2^{∞} periodic orbit. Its fractal and multifractal properties have been studied in great detail [166].

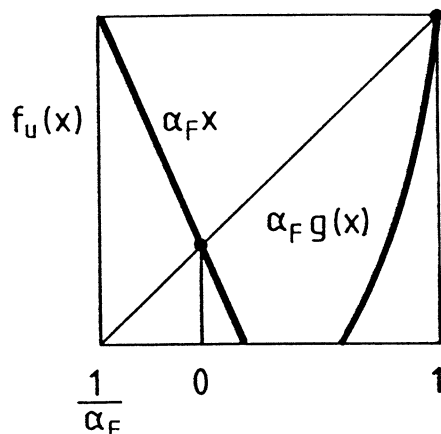


Figure 18: A schematic plot of the universal map f_u the invariant set of which is the period-doubling attractor. In reality, the branch $\alpha_F g(x)$ is much closer to a straight line

It is a relatively recent observation [167, 150] that the attractor as a geometrical object appears also as a *repeller* of a map f_u which can be expressed via universal quantities. This rule follows also from a general theory of renormalization and applies to other universal attractors, too [168]. The function f_u for the quadratic map family consists of a straight line branch $f_u(x) = \alpha_F x$ with $\alpha_F = -2.5029\dots$ being a universal scaling exponent [165] and a somewhat curved branch $f_u(x) = \alpha_F g(x)$. The function f_u is defined on the interval $I = (1/\alpha_F, 1)$ (Figure 18).

The repeller of f_u is geometrically identical with the period doubling attractor. Cylinders generated by the preimages of I provide also a coverage of the attractor. One must, however, be careful when trying to study *metric* properties, since the natural measure of the repeller is not the same as that of the attractor! The natural measure on the attractor is generated by the forward iterates $x_n = g^n(x_0)$ of $x_0 = 1$. It is easy to check that this trajectory visits equally often all cylinders of level n , consequently, the natural measure on the attractor must be the same in all cylinders. Fortunately, this can be interpreted also as an invariant measure on the repeller, namely, the $\sigma = 0$ *Gibbs measure*.

It is, therefore, possible to study the characteristics of the natural measure on the period doubling attractor by means of the methods presented in section 3. The most important quantity is the set of dimensions since entropies and Lyapunov numbers on this attractor belonging to the borderline of chaos are still zero. One might determine the free energy via equation (26) and calculate D_q from relation (36) with $\sigma = 0$. Alternatively, an eigenvalue equation can be written directly for the dimensions of the order 0 Gibbs measure as

$$Q_{n+1}(x') = \bar{e}^{K_0 q} \sum_{x \in f_u^{-1}(x')} \frac{Q_n(x)}{|f'_u(x)|^{(1-q)D_q}}. \quad (95)$$

Since the map has two branches, the topological entropy K_0 of the repeller (in contrast to that of the attractor) is $\ln 2$. By using highly accurate polynomial expansions for $g(x)$, the generalized dimension of the period doubling universal attractor could be determined by this method with ten digits accuracy [62].

It is interesting to note that there exists another eigenvalue equation containing f_u which yields as its highest eigenvalue the other universal exponent δ [165] of the period doubling route to chaos. Based on the observations of [169, 66, 170] the equation can be written as

$$Q_{n+1}(x') = \frac{1}{\delta} \sum_{x \in f_u^{-1}(x')} Q_n(x) f'_u(x). \quad (96)$$

Note that this equation is not of Frobenius-Perron type as the function describing the dynamics appears here without modulus. Nevertheless, it defines an iteration scheme: starting with any smooth and positive initial function convergence sets in only if δ takes on the universal value which can thus be determined very accurately. Equivalently, this can be done also by determining a zeta function based on the primitive cycles of the map f_u [66].

5.2 Models of disordered systems

Renormalization group transformations or, more generally, length scaling or decimation procedures when applied to models of disordered systems often lead to unbounded iterations in the parameter space.

A classical example is provided by the *phonon spectrum of fractals*. Imagine a two-dimensional Sierpinski gasket lattice of point masses linked by identical strings and allowed to move perpendicularly to the plane of the lattice. A decimation procedure applied to frequency ω of the collective motion yields [171] a new frequency $\omega' = \omega(5 - \omega)$. Note, this recursion is equivalent to $x' = 1 - 3.75x^2$ and generates transient chaos. A quantity of central interest is the spectrum of eigenfrequencies. The invariant set of the frequency iteration is obviously part of the spectrum. Thus, each point of the *repeller* represents an element of the vibration spectrum which exhibits, therefore, a *Cantor set structure*. For more detail see [171].

The investigations of quantum properties [172] or dynamical aspects [173, 174] of fractals, as well as certain models of amorphous solids [175], localization [176]-[178] and quasicrystals [179] all lead to (sometimes higher dimensional) recursion relations possessing strange repellers. To illustrate how properties of the repeller can be connected with quantities of solid state physical relevance, we discuss the case of the random field Ising model [180]-[187] in some detail.

5.2.1 Random field Ising chain

Take a semi infinite chain of Ising spins $\{s_1, s_2, \dots, s_n, \dots\}$ in an inhomogenous external field $\{h_1, h_2, \dots, h_n, \dots\}$ with Hamiltonian

$$H = \sum_{j=1}^{\infty} (K s_j s_{j+1} + h_j s_j) \quad (97)$$

where K is a coupling constant. For simplicity we use units in which $k_B T = 1$. The set of local fields $\{h_j\}$ is considered as a particular realization of a random field distribution assuming at each site the values $+h$ and $-h$ with probabilities p and $1 - p$, respectively.

The thermal properties of the system are obtained by evaluating the partition sum

$$Z = \sum_{\{s_1, s_2, \dots\}} \exp(-K s_1 s_2 - h_1 s_1 - \sum_{j=2}^{\infty} (K s_j s_{j+1} + h_j s_j)) \quad (98)$$

at a fixed realization of the fields and averaging the free energy over different realizations afterwards. The summation over spins can be made in a recursive way [180]. Since the first spin appears in two terms of H only, the partial sum is easily obtained in the form

$$Z = \sum_{\{s_2, s_3, \dots\}} 2 \cosh(K s_2 + h_1) \exp(-\sum_{j=2}^{\infty} (K s_j s_{j+1} + h_j s_j)). \quad (99)$$

As s_2 can take on the values ± 1 only, an exponential representation of the cosh function gives:

$$\cosh(K s_2 + h_1) = \exp(A(K, h_1) + g(K, h_1) s_2) \quad (100)$$

where

$$\begin{aligned} A(K, x) &= \frac{1}{2} \ln(\cosh(K + x) \cosh(K - x)), \\ g(K, x) &= \frac{1}{2} \ln(\cosh(K + x) / \cosh(K - x)). \end{aligned} \quad (101)$$

This form shows that spin 1 gives the contribution $-A(K, h_1)$ to the free energy, and generates simultaneously also an extra field $g(K, h_1)$ for spin 2. The partition sum can thus be written as

$$Z = \sum_{\{s_2, s_3, \dots\}} \exp(A(K, h_1)) \exp(-K s_2 s_3 - x_2 s_2 - \sum_{j=3}^{\infty} (K s_j s_{j+1} + h_j s_j)) \quad (102)$$

where x_2 is an effective field acting on spin 2, and is given by

$$x_2 = h_2 + g(K, h_1). \quad (103)$$

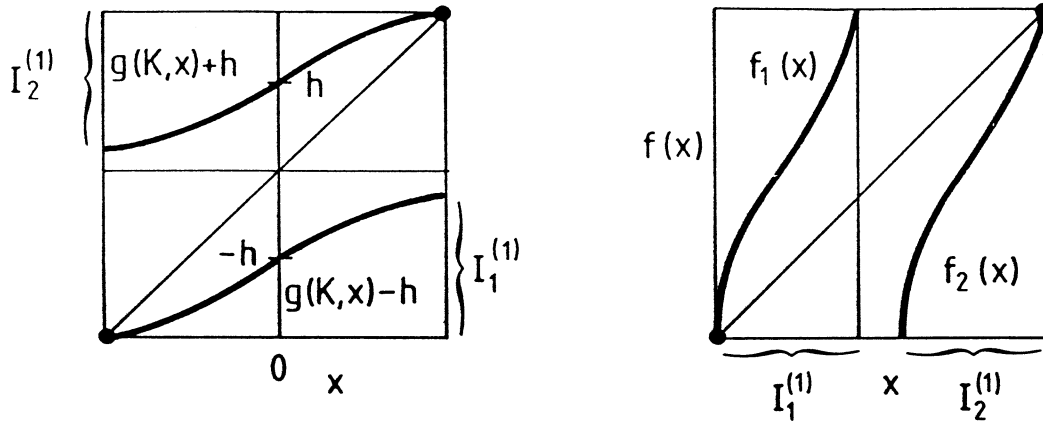


Figure 19: Left: Random map generating the local field x . Right: The inverse of the map. The repeller of this map is the attractor of the random iteration (104) for any choice of the probability p

Note that the partition sum has a similar form to the original one (with x rather than h for spin 2). Hence, the summation over subsequent spins can be carried out in an analogous way. After n steps we find the field acting on spin $(n + 1)$ as

$$x_{n+1} = h_{n+1} + g(K, x_n) \quad (104)$$

and the actual contribution to the free energy will be $-A(K, x_n)$.

Thus, a recursion has been found which is actually a *random* one since the fields $\{h_j\}$ are random variables [181]. According to the field distribution, x_{n+1} takes on the values $h + g(K, x_n)$ and $-h + g(K, x_n)$ with probability p and $1 - p$, respectively. Consequently, the recursion can be written as a *two valued* map in which iterates stay on the upper [lower] branch with probability p [$1 - p$] (see Figure 19). The actual form of the map depends only on the coupling constant K and the field magnitude h . Although the branches alone are not expanding, the random map exhibits chaotic motion on an attractor. The natural invariant measure on this attractor is of great importance since the averaged thermal free energy per spin is just the mean value of $-A(K, x)$ taken with the natural measure of variable x on the attractor. The averaged magnetization per spin and other thermal properties can also be expressed by means of the natural measure [181].

At certain parameter settings there is a gap between the branches as shown on Fig. 19. This has the consequence that the attractor is a *fractal*. One sees immediately that the whole interval I on which the dynamics is defined is mapped then into two smaller ones with the gap in between, and the images of the small intervals will have also holes, in any order. In fact, these intervals are exactly the *cylinders* in the *inverted* map shown on the right of Figure 19. Thus, one concludes

that the attractor of the random map is nothing but the *repeller* of the inverted map [182]. This statement holds for all values of probability p . The natural measure on the attractor, however, depends strongly on the choice of p and is not related to the natural measure of the repeller.

The natural measure of the attractor can, of course, be obtained by iterating the map f backward with branching probabilities p and $1 - p$ and is independent of the choice of initial point. The measure is a multifractal [183, 184]. An efficient way to obtain its D_q spectrum is to solve the eigenvalue equation (41) which takes now the form

$$Q_{n+1}(x) = \sum_{r=1}^2 \frac{Q_n(f_r^{-1}(x)) p_r^q}{|f'(f_r^{-1}(x))|^{(1-q)D_q}} \quad (105)$$

where f is the map shown in Fig. 19 and $p_1 = 1 - p, p_2 = p$.

In the special case $p = 1/2$ the natural measure on the attractor is just the $\sigma = 0$ Gibbs measure of the repeller since all cylinders are equally probable in this case. This is why the order 0 Gibbs measure is often called *balanced* measure. Eq.(105) becomes then equivalent to (95).

It is interesting to note that free energy fluctuations which are due to different realizations of the random field in finite chains are closely related to the multifractal spectrum of the natural measure [184], and similar results can be obtained if magnetic field is not present but the coupling constant K is randomly distributed along the chain [185].

5.3 Irregular scattering

With this last example we leave the field of dissipative phenomena and turn to Hamiltonian systems. We shall study autonomous systems with unbounded energy surfaces in phase space. As a consequence of unboundedness, the majority of trajectories will not stay in a finite region. Since forces generally decay with distance, particles will exhibit a free motion asymptotically. Thus, if chaotic behaviour characterizes such systems at all, it must be transient and must occur in a region where forces are strong enough.

A typical class of unbounded systems is provided by scattering phenomena which are very common in physics. One starts particles in an asymptotic region where interaction is weak, lets them approach a scattering center characterized by strong forces, and asks how particles behave after leaving the scattering center. It is a relatively recent observation that in systems having extended and nontrivial interaction centers, regular scattering is exceptional and irregular or chaotic scattering is typical, in a very much analogous way as integrability and nonintegrability occur in bounded Hamiltonian systems.

What one sees in irregular scattering is that the outgoing trajectories can have very complicated behaviour even in simple systems. This means that the function connecting the properties of outgoing particles with that of the incoming ones displays wild fluctuations which occur on all scales of the incoming parameter. This

phenomenon has been observed in various branches of physics including

- chemical reactions (classical theory) [188],
- celestial mechanics [189],
- fluid dynamics [190]
- and potential scattering [191]-[207].

For reviews see [196, 207]. Unfortunately, no experimental evidence has been reported yet.

To be more specific, here we take the simplest class of systems exhibiting irregular behaviour, that of potential scattering in two-dimensions. Particles move then in a fixed potential $V(x, y) > 0$ which falls off sufficiently fast for large values of the coordinates. The quantity of central interest is the deflection function telling us how the angle difference between incoming and outgoing directions depends on the impact parameter at a given incidence angle. It has been found [192]-[203] that although this function has smooth pieces, in certain regions it varies rapidly. Moreover, such regions contain points where the function is not defined at all, and these points lie on a fractal set, i.e. the behaviour is repeated on all scales. A comparison with the time spent in the interaction center shows that the delay time diverges exactly in points where the deflection function is undefined (Fig. 20).

Thus, one concludes that trajectories can be *trapped* in the interaction region. The initial conditions for such trajectories sit on a fractal. They are therefore directly not observable but so are trajectories which get close to the trapped ones. It has also been shown [192, 193] that trajectories are trapped by bounded *hyperbolic periodic orbits* lying inside the scattering region, along their stable manifolds. Consequently, there exists a *chaotic repeller* (remember: fractality implies transient chaos) which is practically the set of all unstable cycles, and is responsible for the irregular, chaotic behaviour. This is consistent also with the observation that the average lifetime inside the interaction region follows an exponential decay [195].

The properties of the repeller can be studied by methods described earlier. It is worth defining a Poincaré plane, say by taking intersections with the $y = 0$ axis and keeping x, p_x or x, θ (θ : direction of momentum p) as variables after eliminating others by use of energy conservation. Chaotic repellers have been identified by using the horseshoe construction [196, 205] (Fig. 21) and the PIM triple procedure [203] (Fig. 22). It is worth noting that due to the reversibility of the motion, stable and unstable manifolds are obtained by simple reflections in Hamiltonian systems.

When turning to metric properties of irregular scattering, the natural measure is to be identified. Since one deals with a similar repeller as before, the *same* natural measure has to be taken as for dissipative cases [56], i.e. the measure defined by long lived (in our case trapped) trajectories around the repeller. This measure has not been constructed numerically, but its characteristics can be derived also without construction. We can use relations of section 4. Note first that the Jacobian in Hamiltonian systems is uniformly 1. Consequently, the free energy provides a complete characterization of the scaling properties. A comparison of (59)

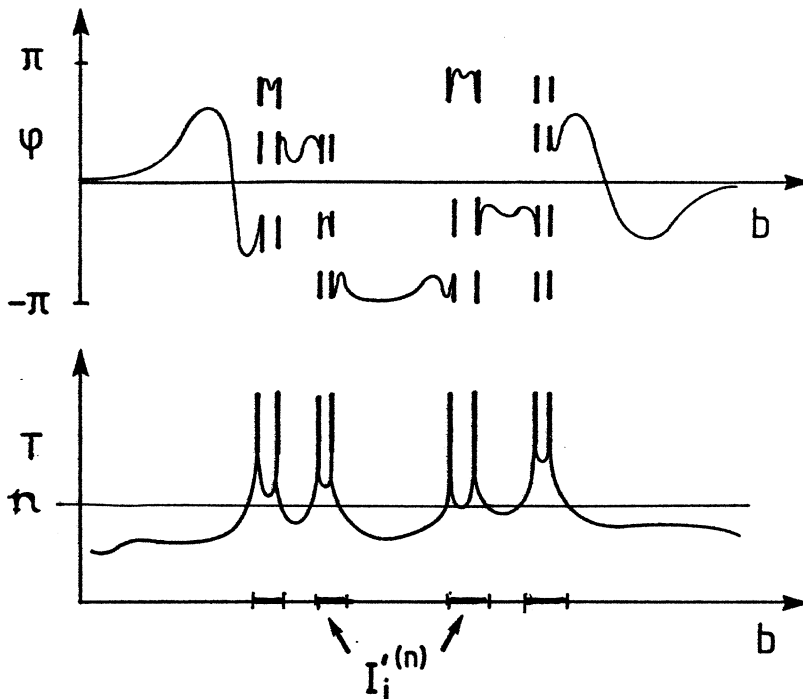


Figure 20: Schematic plot of the angle deflection φ and the delay time T versus the impact parameter b for chaotic scattering. Particles started in the intervals $I_i^{(n)}$ have at least n collisions inside the scattering center. For $n \rightarrow \infty$ they cover the fractal on which the singularities in φ and T sit

and (80) leads to the conclusion that

$$D_q^{(1)} = D_q^{(2)}, \quad (106)$$

i.e. Hamiltonian repellers are *isotropic* multifractals [56]. The fact that the fractal dimensions agree follows already from the symmetry between stable and unstable manifolds. Particular values of the Lyapunov exponents, entropies or partial dimensions are obtained via relations (19),(24) and (59), respectively, provided the free energy is known.

The free energy can be specified either via calculating a zeta function [66] or by measuring the length scales $\epsilon_i^{(n)}$ in a generating partition. The latter method can be simplified observing that the dynamics only slightly distorts intervals when carrying them along the stable manifolds of the repeller. Therefore, we can do the following [204]. Take a straight line far away from the repeller. It intersects the stable manifolds in a fractal set. Specify next intervals $I_i^{(n)}$ from which trajectories do not leave a neighbourhood D of the repeller before n steps. For n large enough, these intervals are practically the intersections of the straight line with the n th preimage of D . Since stable manifolds extend smoothly to infinity, the lengths $l_i^{(n)}$

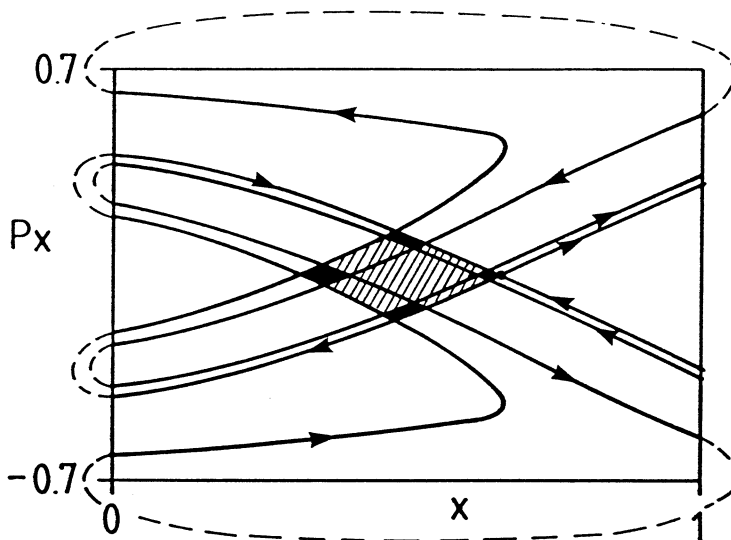


Figure 21: Stable and unstable manifolds of a periodic orbit (marked by a dot) in a potential consisting of three identical Gaussian hills concentrated on the vertices of a regular triangle [205]. The hatched area contains the repeller, double hatched regions provide a coverage of it. Dashed lines show topological connections of manifolds

of intervals $I_i^{(n)}$ are proportional to those in the generating partition $(\epsilon_{1i}^{(n)})$. Thus, one finds the free energy also via the scaling relation

$$\sum_i l_i^{(n)\beta} \sim e^{-\beta F(\beta)n}. \quad (107)$$

Furthermore, since the motion in phase space and in the Poincaré map is connected by a smooth transformation, the same relation holds for lengths l' of intervals I' defined in the coordinate space [204]: Take a straight line far away from the interaction region and start trajectories from it in a given direction (with constant velocity). Those which do not leave the interaction region up to n collisions start out from intervals $I_i^{(n)}$ which can be found on a time delay plot, too (Fig. 20). The free energy thus can also be obtained from the partition sum built up by the lengths $l_i^{(n)}$. The use of relation (107) provides a powerful method for deducing the scaling properties of chaotic scattering in two degrees of freedom systems [204, 205].

Finally, two remarks are in order.

Chaos in bounded dissipative and conservative systems exhibits qualitatively different behaviour: there is no analogue of an attractor in Hamiltonian cases. This is not so for repellers. In fact, transient chaos seems to be much more in common in dissipative and conservative cases. Furthermore, chaotic horseshoes are always present locally in bounded Hamiltonian systems. Transient chaos is simpler than permanent one since in the former there is no feedback from trajectories having left the repeller; the horseshoe is isolated.

A particularly attractive feature of chaotic scattering is its quantisability in a direct way which distinguishes it from dissipative cases. The first steps along this

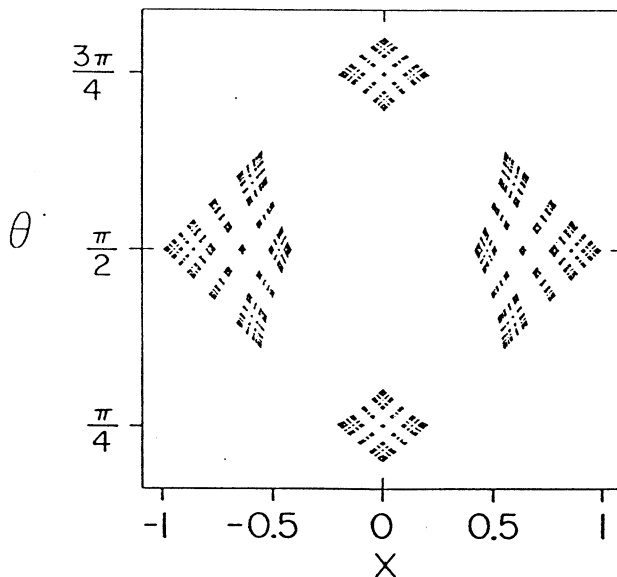


Figure 22: Chaotic repeller in a scattering problem defined by four identical Gaussian hills concentrated on the vertices of a square, obtained by means of the PIM triple method [203]. Compare with a dissipative repeller (e.g., Fig. 4)

line have been taken [195],[208]-[212], and one hopes from this research a better understanding of scattering processes at least on a semiclassical level.

6 Discussion

There are several further aspects of transient chaos not mentioned in the main text. We would like briefly to discuss a few of them here.

As for the methodology, the calculation of *power spectra* [136, 95] can be useful for deciding if signals are transiently chaotic or not. Of course, only the random looking part of signals are to be taken into account. The finite duration is more essential now than in permanent chaotic cases, but there exist algorithms [213] which overcome this problem. A broadband spectrum is a definite sign of chaos. One might speculate about the application of the *time delay* method [214, 122, 136] for reconstructing the dynamics around repellers from time series. The analogues of *truncated* trajectories, as described in section 2.2, are to be used in the analysis which can yield global dimensions or entropies. Also *correlation functions* contain useful information about the system. A sufficiently long signal around a chaotic repeller generates an *exponentially* decaying correlation function which behaves as c^n ($c < 1$) in discrete time [57]. The correlation coefficient c is a characteristic of the chaotic transients and seems to be independent of the thermodynamic quantities introduced earlier.

The phenomenon of *intermittency* has not yet been mentioned in transient context. We note first, there are repellers generating intermittent signals, the transient part of which is characterized by long intervals of approximately periodic behaviour

interrupted by chaotic bursts [61]. Another related phenomenon is *crisis induced intermittency* occurring at sudden widening of chaotic attractors [34] induced by an interior crisis [13]. The signal then exhibits an intermittent bursting out of the phase space region within which the attractor was confined before crisis. In this case a permanent switching between two different kinds of chaotic behaviour takes place which is easily accessible experimentally [75, 80, 81]. The time between bursts into the new widened region has a characteristic length. Its reciprocal value can be considered as the escape rate from the attractor existing before crisis, and was shown to follow scaling law (42) with critical exponent as given by (47) or (48) [26, 34]. In general, we can say that the concept of transient chaos can usefully be applied to analyzing *parts* of chaotic attractors [52, 215].

Julia sets [140], [17], [144], [216]-[219] provide an important class of repellers not yet treated. The reason is that Julia sets appear in *noninvertible* two-dimensional maps, therefore, the analysis of section 4 does not apply to them. In fact, Julia sets of analytic complex recursions have very much in common, in certain parameter range, with repellers of one-dimensional maps and have been investigated in this spirit [144, 217, 219]. Note, since Julia sets are typically generated by a random backward iteration with equal probability for all preimages, the measure obtained in this way is not the natural one but rather the balanced (or order 0 Gibbs) measure.

Transient chaos plays an essential role in *weakly dissipative* nonlinear systems. When dissipation is added to conservative systems, stable orbits become attracting sinks, invariant tori are destroyed and persistent chaotic motion completely disappears. Certain horseshoes, however, survive and are responsible for transient chaotic behaviour [7, 71, 10, 21, 36]. This phenomenon might be relevant also in celestial mechanics.

It is worth noting that in the realm of *Hamiltonian* systems there are, as well as scattering problems, other examples connected with transient chaos. Imagine e.g. a billiard table with a small hole. If the ball can fall through the hole, chaotic motion is restricted to finite time scales [5, 106]. Another example can be the ionization of highly excited atoms in microwave fields [220] which is subject of extensive theoretical and experimental investigation. To analyse also such driven cases in a similar spirit as irregular potential scattering would be desirable.

Let us mention further aspects of practical relevance. One is the influence of *finite precision* on measured quantities, like e.g., escape rate [221]. Another is the *effect of noise* on transient behaviour, and its relation to noise induced chaos [113]. A third problem is the influence of the *adiabatic variation of the system's parameters* on the transients [222]. A systematic study of these subjects is still lacking.

Several open problems are connected with the *nonhyperbolicity* of strange repellers. We saw that chaotic repellers are often hyperbolic. This does not mean, however, that nonhyperbolic cases would be exceptional. The main reasons for nonhyperbolicity are *homoclinic tangencies* (very likely just beyond crisis) or the existence of *marginally stable* orbits on the repeller (occurring, e.g., in one-dimensional maps having a unit slope at the left corner). In Hamiltonian systems invariant tori

around repellers can induce marginal cycles.

In nonhyperbolic cases the natural measure of certain boxes is anomalously high, i.e. *not* proportional to the box size, and/or certain box sizes do *not* scale exponentially with the refinement. Consequently, nonanalytic behaviour, so-called phase transitions, will show up in the thermodynamic functions or in the λ_q, D_q, K_q spectra, just like for chaotic attractors [223, 30, 33, 149], [224]-[231]. Nevertheless, what we learned about hyperbolic repellers remains partially applicable. One expects to find a *range* in parameters β or q , the hyperbolic phase, where the contribution of anomalous boxes is negligible and the system behaves as *if it were hyperbolic*. The behaviour in the complementary, nonhyperbolic phase is, however, still unexplored.

Finally, we comment on *higher dimensional* (hyperbolic) cases. Besides the qualitative picture, also the quantitative relations of section 4 remain valid, if there is one positive Lyapunov exponent and the repeller fills the direction of least contraction only. In cases with more positive Lyapunov exponents the properties of the conditionally invariant measure can be worked out relatively easily [163] as this measure is smooth along unstable manifolds. A detailed thermodynamic description of the natural measure (with fractal properties also in unstable directions) would require a multivariate thermodynamic potential, a generalization of $G(p, \beta)$, in the construction of which cycle eigenvalues could be of great help [66, 68].

We mentioned already that chaotic transients may be a pervasive feature when higher dimensional dynamical behaviour is present [26, 34]. This is consistent with experiments on fluids [70, 73] and with simulations of some partial differential equations [25] and coupled map lattices [35, 232]. The latter shows that the average lifetime of spatially chaotic behaviour grows rapidly with the system's size i.e. with the number of degrees of freedom. Thus, one might speculate about the possibility that strange repellers can be more relevant in certain hydrodynamic phenomena than attractors. Whether this is realistic is not yet known, but clearly the study of chaotic transients in higher dimensional and spatially extended systems deserves more attention.

7 Acknowledgments

The author benefitted greatly from contact with a large number of colleagues. In particular, he would like to express his gratitude to R.Badii, J.Bene, T.Bohr, A.Csordás, P.Cvitanović, F.Drepper, B.Eckhardt, G.Eilenberger, M.Feigenbaum, M.Franaszek, P.Grassberger, C.Grebogi, B.L.Hao, B.Huberman, C.Jung, Z.Kaufmann, A.Kleczkowski, P.M.Koch, Z.Kovács, I.Procaccia, D.Rand, P.Richter, P.Ruján, L.Sasvári, F.Schütte, U.Smilansky, R.Stinchcombe, G.Szabó, P.Szépfałusy, and G.Vattay, for illuminating discussions on the subject. Special thanks go to the authors of Ref. [205] and [203] for the permission to reproduce Figure 21 and 22, respectively. The kind hospitality at the IFF of the KFA Jülich is acknowledged.

References

- [1] J.L.Kaplan and J.A.Yorke, *Comm. Math. Phys.* **67**, 93 (1979)
- [2] J.A.Yorke and E.D.Yorke, *J. Stat. Phys.* **21**, 263 (1979)
- [3] T.Shimizu and N.Morioka, *Phys. Lett.* **69 A**, 148 (1978)
- [4] P.Holmes, *Philos.Trans.R.Soc.London A* **292**, 419 (1979)
- [5] G.Pianigiani and J.A.Yorke, *Trans. Am. Math. Soc.* **252**, 351 (1979);
G.Pianigiani, *J.Math.Anal.Appl.***82**, 75 (1981)
- [6] R.Daveney and Z.Nitecki, *Comm.Math.Phys.* **67**, 137 (1979)
- [7] J.McLaughlin, *Phys.Rev. A* **20**, 2114 (1979)
- [8] J.Coste, *J. Stat. Phys.* **23**, 512 (1980)
- [9] D.A.Russell and E.Ott, *Phys.Fluids* **24**, 1976 (1981)
- [10] B.A.Huberman, *Transient behavior of weakly dissipative dynamical systems*, unpublished preprint (1981)
- [11] D.Ruelle, *Ergod. Theor. Dyn. Syst.* **2**, 99 (1982)
- [12] P.Manneville, *Phys. Lett.* **90 A**, 327 (1982)
- [13] C.Grebogi, E.Ott and J.A.Yorke, *Phys. Rev. Lett.* **48**, 1507 (1982);
Physica D **7**, 181 (1983)
- [14] P.Holmes and D.Whitley, *Physica D* **7**, 111 (1983);
B.D.Greenspan and P.Holmes, in *Nonlinear Dynamics and Turbulence*, eds.:
G.I.Barenblatt, G.Ioos, D.D.Joseph (Pitman,Boston,1983)
- [15] H.McCluskey and A.Manning, *Ergod. Theor. Dyn. Syst.* **3**, 251 (1983)
- [16] C.Grebogi, E.Ott and J.A.Yorke, *Phys. Rev. Lett.* **50**, 935 (1983)
- [17] M. Widom, et al., *J. Stat. Phys.* **32**, 443 (1983)
- [18] L.P. Kadanoff and C. Tang, *Proc. Natl. Acad. Sci. USA* **81**, 12 (1984)
- [19] H.Kantz and P.Grassberger, *Physica D* **17**, 75 (1985)
- [20] C.Grebogi, E.Ott and J.A.Yorke, *Ergod. Theor. Dyn. Syst.* **5**, 341 (1985)
- [21] M.A.Lieberman and K.Y.Tsang, *Phys. Rev. Lett.* **55**, 908 (1985);
K.Y.Tsang and M.A.Lieberman, *Physica D* **21**, 401 (1986)
- [22] S.Takesue, *Prog. Theor. Phys.* **76**, 11 (1986)

- [23] P.Szépfalusy and T.Tél, Phys.Rev. A **34**, 2520 (1986)
- [24] J.M.Hyman, B.Nicolaenko and S.Zaleski, Physica D **23**, 265 (1986)
- [25] B.I.Shraiman, Phys. Rev. Lett. **57**, 325 (1986)
- [26] C. Grebogi, E.Ott and J.A.Yorke, Phys. Rev. Lett. **57**, 1284 (1986)
- [27] T.Tél, Phys. Lett. **119 A**, 65 (1986)
- [28] V.G.Benza and S.W.Koch, Phys.Rev. A **35**, 174 (1987)
- [29] T.Bohr and D.Rand, Physica D **25**, 387 (1987);
D.Rand, *The singularity spectrum of hyperbolic Cantor sets and attractors*, unpublished preprint, 1986
- [30] P.Szépfalusy and T.Tél, Phys.Rev. A **35**, 477 (1987)
- [31] T.Tél, Phys.Rev. A **36**, 1502 (1987)
- [32] P.Smereka, B.Birnir and S.Banerjee, Phys.Fluids **30**, 3342 (1987)
- [33] T.Tél, Phys.Rev. A **36**, 2507 (1987)
- [34] C.Grebogi, E.Ott, F.Romeiras and J.A.Yorke, Phys.Rev. A **36**, 5365 (1987)
- [35] J.P.Crutchfield and K.Kaneko, in *Directions in Chaos*, Vol.I, ed.: Bai-lin Hao (World Scientific, Singapore, 1987)
- [36] F.M.Izrailev, B.Timmermann and W.Timmermann, Phys. Lett. **126 A**, 405 (1988)
- [37] B.P.Koch and B.Bruhn, J.Physique **49**, 35 (1988)
- [38] S.Vaianti, J. Phys. A **21**, 2023; 2313 (1988)
- [39] D.Bessis, G.Paladin, G.Turchetti and S.Vaianti, J. Stat. Phys. **51**, 109 (1988)
- [40] M.Mareyen and F.J.Schütte, Potsdamer Forschung **B64**, (1988)
P.Belkner et al., in *Quantum Optics* (World Scientific, Singapore, 1988)
- [41] T.Bohr and T.Tél, in *Directions in Chaos*, Vol. II, ed.: U. Bai-lin Hao, (World Scientific, Singapore, 1988)
- [42] G.Hsu, E.Ott and C.Grebogi, Phys. Lett. **127 A**, 199 (1988)
- [43] G.Turchetti and S.Vaianti, Phys. Lett. **128 A**, 343 (1988)
- [44] O.B.Christensen and T. Bohr, Physica Scripta **38**, 641 (1988)
- [45] B.Pompe and R.Leven, Physica Scripta **38**, 651 (1988)
- [46] T.Yoshida and B.C.So, Prog. Theor. Phys. **79**, 1 (1988)

- [47] K.J.Falconer, J. Phys. A **21**, L737 (1988)
- [48] P.Cvitanović, Phys. Rev. Lett. **61**, 2729 (1988)
- [49] D.Rand, Ergod. Theor. Dyn. Syst. **9**, 527 (1989)
- [50] J.M.T.Thompson, Proc.Roy.Soc.Lond.A **421**, 195 (1989)
- [51] J.Bene, Phys.Rev. A **39**, 2090 (1989)
- [52] H.E.Nusse and J.A.Yorke, Physica D **36** 137 (1989)
- [53] E.Ott, T.Sauer and Y.Yorke, Phys.Rev. A **39**, 4212 (1989)
- [54] D.K.Umberger, C.Grebogi, E.Ott and B.Afeyan, Phys.Rev. A **39**, 4835 (1989)
- [55] O.Biham and W.Wenzel, Phys. Rev. Lett. **63**, 819 (1989)
- [56] T.Tél, J. Phys. A **22**, L691 (1989)
- [57] A.Csordás, Thesis, Budapest, 1989 (in Hungarian)
- [58] Bai-lin Hao, *Elementary Symbolic Dynamics and Chaos in Dissipative Dynamical Systems*, Chapter 7 (World Scientific, Singapore, 1989)
- [59] O.E.Rössler and J.L.Hudson, in *Chaotic Dynamics in Brain Function*, eds.: E.Basar, T.H.Bullock (Springer, Berlin, 1989)
- [60] K.Germey, F.J.Schütte and R.Tiebel, Opt.Comm. **69**, 438, (1989)
- [61] Z.Kaufmann, Thesis, Budapest, 1989 (in Hungarian); and unpublished
- [62] Z.Kovács, J. Phys. A **22**, 5161 (1989)
- [63] R.Badii and G.Broggi, in *Quantitative Measures of Dynamical Complexity in Non-linear Systems*, eds.: N.B.Abraham, A.Albano (Plenum, New York, 1990)
- [64] B.A.Huberman and E.Lumer, IEEE Transactions on Circuits and Systems, to appear
- [65] H.E.Nusse and J.A.Yorke, Ergod. Theor. Dyn. Syst. , to appear
- [66] R.Artuso, E.Aurell and P.Cvitanović, Nonlinearity, to appear
- [67] T.Yoshida and S.Miyazaki, Prog.Theor.Phys.Suppl., to appear
- [68] P.Cvitanović, in *Nonlinear Physical Phenomena*, eds.: A.Ferraz, F.Oliveira and R.Osorio (World Scientific, Singapore, 1990);
P.Cvitanović and B.Eckhardt, to be published

- [69] W.M.Schaffer et al., in *From Chemical to Biological Organization*, ed.: M.Markus et al, (Springer,Berlin,1987);
F.R.Drepper, in *Ecodynamics*, eds.: W.F.Wolff et al., (Springer, Berlin,1988);
F.Drepper, J.McGlade and D.Rand, *The unpredictability profile of measles incidence pattern*, preprint, 1990
- [70] G.Ahlers and R.W.Walden, Phys. Rev. Lett. **44**, 445 1980
- [71] V.Croquette and C.Poitou, C.R.Acad.Sc.Paris**292**, 1353 (1981)
- [72] F.T.Arecchi, R.Meucci, G.Puccioni and J.Tredicce, Phys. Rev. Lett. **49**, 1217 (1982)
- [73] P.Bergé and M.Dubois, Phys. Lett. **93 A**, 365 (1983)
- [74] F.T.Arecchi and F.Lisi, Phys. Rev. Lett. **50**, 1330 (1983)
- [75] R.W.Rollins and E.R.Hunt, Phys.Rev. **A 29**, 3327 (1984);
R.C.Hilborn, Phys.Rev. **A 31**, 378 (1985)
- [76] R.W.Leven, B.Pompe, C.Wilke and B.P.Koch, Physica **D 16**, 371 (1985)
- [77] M.Gorman, P.J.Widmann and K.A.Robbins, Phys. Rev. Lett. **52**, 2241 (1984);
Physica **D 19**, 255 (1986);
P.J.Widmann, M.Gorman and K.A.Robbins, Physica **D 36**, 157 (1989);
For an early attempt see: H.F.Creveling et al., J.Fluid.Mech.**67**, 65 (1975)
- [78] T.L.Carroll, L.M.Pecora and F.J.Rachford, Phys. Rev. Lett. **59**, 2891 (1987);
Phys.Rev. **A 40**, 377; 4149 (1989); J.Appl.Phys. **64**, 5396, (1988);
T.L.Carroll, F.J.Rachford and L.M.Pecora, Phys.Rev. **B 38**, 2938 (1988)
- [79] Z.J.Kowalik, M.Franaszek and P.Pieranski, Phys.Rev. **A 37**, 4016 (1988)
- [80] F.Papoff, D.Dangoisse, E.Poite-Hanoteau and P.Glorieux, Optics Comm. **67**, 358 (1988);
D.Dangoisse, P.Glorieux and D.Hennequin, Phys. Rev. Lett. **57**, 2657 (1986)
- [81] W.L.Ditto et al., Phys. Rev. Lett. **63**, 923 (1989)
- [82] T.Riste and K.Otnes, Z. Phys. **B 77**, 471 (1989);
K.Otnes and T.Riste, to be pulished
- [83] C.Grebogi, S.W.McDonald, E.Ott and J.A.Yorke, Phys. Lett. **99 A**, 415, (1983)
- [84] S.Takesue and K.Kaneko, Prog. Theor. Phys. **71**, 35 (1984)
- [85] R.G.Holt and I.B.Schwartz, Phys. Lett. **105 A**, 327 (1984);
I.B.Schwartz, Phys. Lett. **106 A**, 339 (1984)
- [86] S.W. McDonald, C. Grebogi, E. Ott and J.A. Yorke, Physica **D 17**, 125 (1985);
Phys. Lett. **107 A**, 51 (1985)

- [87] E.G.Gwinn and R.M.Westervelt, Phys. Rev. Lett. **54**, 1613 (1985)
- [88] Y.Yamaguchi and Mishima, Phys. Lett. **109 A**, 196 (1985);
Y.Yamaguchi and K.Tanikawa, Phys. Lett. **117 A**, 450 (1986)
- [89] M.Iansiti, Q.Hu, R.M.Westervelt and M.Tinkham, Phys. Rev. Lett. **55**, 746 (1985)
- [90] F.T.Arecchi, R.Badii and A.Politi, Phys.Rev. **A 32**, 402 (1985)
- [91] F.C.Moon and G.X.Li, Phys. Rev. Lett. **55**, 1439 (1985)
- [92] E.G.Gwinn and R.M.Westervelt, Phys.Rev. **A 33**, 4143 (1986); Physica **D 23**, 396 (1986)
- [93] C.Grebogi, E.Ott and J.A.Yorke, Phys. Rev. Lett. **56**, 1011 (1986); Physica **D 24**, 243 (1987)
- [94] J.S.Nicolis, Rep.Prog.Phys.**49**, 1109 (1986)
- [95] F.C.Moon, *Chaotic Vibrations* (Wiley, New York, 1987)
- [96] C.Grebogi, E.Kostelich, E.Ott and J.A.Yorke, Phys. Lett. **118 A**, 448 (1986); Physica **D 25**, 347 (1987)
- [97] C.Pezeshki and E.H.Dowell, J.Sound Vibr. **117**, 219 (1987)
- [98] L.Kocarev, Phys. Lett. **121 A**, 274 (1987); Phys. Lett. **125 A**, 389 (1987)
- [99] J.M.T.Thompson, S.R.Bishop and L.M.Leung, Phys. Lett. **121 A**, 116 (1987)
- [100] J.M.Aguirregabiria and J.R.Etxebarria, Phys. Lett. **122 A**, 241 (1987)
- [101] C.Grebogi, E.Ott and J.A.Yorke, Science **238**, 585 (1987)
- [102] M.Napiórkowski and S.Thomae, Europhys.Lett. **4**, 1247 (1987)
- [103] C.Grebogi, H.Nusse, E.Ott and J.A.Yorke, Lect.Notes in Math. **1342**, 220, (1988);
P.M.Battelino, C.Grebogi, E.Ott and J.A.Yorke, Physica **D 32**, 296 (1988)
- [104] M.Varghese and J.S.Thorp, Phys. Rev. Lett. **60**, 665 (1988)
- [105] H.M.Isomäki, J.von Boehm and R.Räty, Phys. Lett. **126 A**, 484 (1988)
- [106] S.Bleher, C.Grebogi, E.Ott and R.Brown, Phys.Rev. **A 38**, 930 (1988)
- [107] Y.Yamaguchi et al., Phys. Lett. **128 A**, 470 (1988);
Y.Yamaguchi, Phys. Lett. **135 A**, 259 (1989);
Y.Yamaguchi and K.Tanikawa, Phys. Lett. **142 A**, 95 (1989)
- [108] B.Park, C.Grebogi, E.Ott and J.A.Yorke, Phys.Rev. **A 40**, 1576 (1989)
- [109] K.Aoki and N.Mugibayashi, Appl.Phys.A **48**, 161 (1989)

- [110] O.E.Rössler, J.L.Hudson and M.Klein, *J.Phys.Chem.* **93** 2858 (1989);
O.E.Rössler, J.L.Hudson, M.Klein and C.Mira, in *Nonlinear Dynamics in Engineering*, ed.: W.Schiehlen, (Springer,Berlin,1989)
- [111] H.M.Isomäki, in *Nonlinear Dynamics in Engineering*, ed.: W.Schiehlen,
(Springer,Berlin,1989)
- [112] F.T.Arecchi, R.Badii and A.Politi, *Phys.Rev. A* **29**, 1006 (1984)
- [113] R.L.Kautz, *J.Appl.Phys.* **58**, 424 (1985)
- [114] H.Herzel, W.Ebeling and T.Schulmeister, *Z.f.Naturforsch.* **42a**, 136 (1987)
- [115] V.S.Anishchenko and H.Herzel, *Z.angew.Math.Mech.* **68**, 317 (1988)
- [116] S. Smale, *Bull. Am. Math. Soc.* **73**, 747 (1967)
- [117] J.Guckenheimer and P.Holmes, *Nonlinear Oscillations, Dynamical Systems, and Bifurcations of Vector Fields*, (Springer, Berlin, 1983)
- [118] I.Procaccia, *Nature* **333**, 618 (1988)
- [119] A.B.Katok, *Publ.Math.IHES* **51**, 137 (1980)
- [120] H.Fujisaka, *Prog. Theor. Phys.* **70**, 1264 (1983); **71**, 513 (1984) **38a**, 1157 (1983)
- [121] R.Benzi, G.Paladin, G.Parisi and A.Vulpiani, *J. Phys. A* **18**, 2157 (1985)
- [122] P.Grassberger, in *Chaos*, ed.: A.V.Holden (Manchester Univ. Press, Manchester, 1986)
- [123] R. Badii and A. Politi, *Phys.Rev. A* **35**, 1288 (1987); *Physica Scripta* **35**, 243 (1987)
- [124] P. Grassberger, R. Badii and A. Politi, *J. Stat. Phys.* **51**, 135 (1988)
- [125] A.Rényi, *Probability Theory*, (North-Holland,Amsterdam, 1970)
- [126] B.B.Mandelbrot, *J.Fluid.Mech.***62**, 331 (1974)
- [127] K.Kaplan and J.Yorke, *Lect.Notes in Math.* **730**, 228 (1979)
- [128] L.S.Young, *Ergod. Theor. Dyn. Syst.* **2**, 109 (1982)
- [129] B.B.Mandelbrot, *The Fractal Geometry of Nature*, (Freeman, San Francisco, 1982)
- [130] H.G.E.Hentschel and I.Procaccia, *Physica D* **8**, 435 (1983)
- [131] P. Grassberger and I. Procaccia, *Physica* **13D**, 34 (1984);
F.Ledrappier, L.S.Young, *Ann.Math.* **122**, 509; 540 (1985)
- [132] P.Grassberger, *Phys. Lett.* **97 A**, 227 (1983); *Phys. Lett.* **107 A**, 101 (1985)

- [133] U.Frisch and G.Parisi, in *Turbulence and Predictability in Geophysical Fluid Dynamics and Climate Dynamics*, eds.: N.Ghil et al., (North-Holland, Amsterdam, 1985)
- [134] T.C.Halsey, et al., *Phys.Rev. A* **33**, 1141 (1986)
- [135] P. Grassberger and I. Procaccia, *Phys.Rev. A* **28**, 2591 (1983):
- [136] J.P. Eckmann and D. Ruelle, *Rev. Mod. Phys.* **67**, 617 (1985)
- [137] J.P. Eckmann and I. Procaccia, *Phys.Rev. A* **34**, 659 (1986)
- [138] Y.G.Sinai, *Usp.Mat.Nauk.* **27**, 21 (1972) [*Russ.Math. Surveys* **166**, 21 (1972)]
- [139] R.Bowen, *Lect.Notes in Math.* **470**, 1 (1975)
- [140] D. Ruelle: *Thermodynamic Formalism* (Addison-Wesley, Reading,1978)
- [141] D.H.Mayer, *Lect.Notes in Phys.* **123**, 1 (1980)
- [142] D.Ruelle, *Phys. Rev. Lett.* **56**, 405 (1986); *J. Stat. Phys.* **56**, 405 (1986)
- [143] M.J.Feigenbaum, M.H.Jensen and I.Procaccia, *Phys. Rev. Lett.* **56**, 1503 (1986)
- [144] M.H.Jensen, L.P.Kadanoff and I.Procaccia, *Phys.Rev. A* **36**, 1409 (1987)
- [145] M.J.Feigenbaum, *J. Stat. Phys.* **46**, 919; 925 (1987)
- [146] M.Kohmoto, *Phys.Rev. A* **37**, 1345 (1987)
- [147] P.Alström, in *Time-Dependent Effects in Disordered Materials*, eds.: R.Pynn and T.Riste (Plenum, New York, 1987)
- [148] M.J.Feigenbaum, in *Nonlinear Evolution and Chaotic Phenomena*, eds.:G.Galavotti and P.F.Zweifel, (Plenum, New York, 1988)
- [149] A.Csordás and P.Szépfolusy, *Phys.Rev. A* **38**, 2582 (1988)
- [150] M.J.Feigenbaum, *J. Stat. Phys.* **52**, 527 (1988)
- [151] T.Tél, *Z.f.Naturforsch.* **43a**, 1154 (1988)
- [152] R.Badii, *Riv.Nouv.Cim.* **12**, N3, 1 (1989)
- [153] M.J.Feigenbaum, I.Procaccia and T.Tél, *Phys.Rev. A* **39**, 5359 (1989)
- [154] J.L.McCauley, *Int.J.Mod.Phys.* **3**, 821 (1989)
- [155] Z.Kovács and T.Tél, *Phys.Rev. A* **40**, 4641 (1989)
- [156] A.B.Chhabra, R.V.Jensen and K.R.Sreenivasan, *Phys.Rev. A* **40**, 4593, 1989

- [157] T.Tél, J. Stat. Phys. **33**, 195 (1983);
K.G.Szabó and T.Tél, J. Stat. Phys. **54**, 925 (1989)
- [158] D. Auerbach, P. Cvitanovic, J.P. Eckmann, G.H. Gunaratne and I. Procaccia, Phys. Rev. Lett. **58**, 2387 (1987)
- [159] T. Kai and K. Tomita, Prog. Theor. Phys. **64**, 1532 (1980);
Y. Takahashi and Y. Oono, Prog. Theor. Phys. **71**, 851 (1984) 1077 (1987)
- [160] G.H. Gunaratne and I. Procaccia, Phys. Rev. Lett. **59**, 1377 (1987);
D. Auerbach, B. O'Shaughnessy and I. Procaccia, Phys. Rev. A **37**, 2234 (1988);
G.H. Gunaratne, M.H. Jensen and I. Procaccia, Nonlinearity **1**, 157 (1988);
P. Cvitanović, G.H. Gunaratne and I. Procaccia, Phys. Rev. A **38**, 1503 (1988)
- [161] T. Morita et al., Prog. Theor. Phys. **78**, 511 (1987);
H. Hata et al., Prog. Theor. Phys. **78**, 721 (1987)
- [162] C. Grebogi, E. Ott and J.A. Yorke, Phys. Rev. A **36**, 3522 (1988)
- [163] C. Grebogi, E. Ott and J.A. Yorke, Phys. Rev. A **37**, 1711 (1988)
- [164] P.Grassberger, H.Kantz and U.Moenig, J. Phys. A **22**, 5217 (1989)
- [165] M.J.Feigenbaum, J. Stat. Phys. **21**, 669 (1979)
- [166] P.Grassberger, J. Stat. Phys. **26**, 173 (1981)
D.Bensimon, M.H.Jensen and L.P.Kadanoff, Phys.Rev. A **33**, 3622 (1986)
E.Aurell, Phys.Rev. A **34**, 5135 (1986); Phys.Rev. A **35**, 4016 (1987);
C.Beck, Physica D, to appear
- [167] F.Ledrappier and M.Misiurewicz, Ergod. Theor. Dyn. Syst. **5**, 595 (1985);
P.Collet, J.Lebowitz and A.Porzio, J. Stat. Phys. **47**, 609 (1987)
- [168] D.Rand, Nonlinearity **1**, 181 (1988)
- [169] D.Sullivan, in *Universality in Chaos*, 2nd Edition, ed.: P.Cvitanović (Adam Hilger, Bristol, 1989)
- [170] Z.Kovács, private communication
- [171] R.Rammal and G.Toulouse, J.Physique Lett. **44**, L13 (1983);
R.Rammal, J.Physique **45**, 191 (1984)
- [172] E.Domany, S.Alexander, D.Bensimon and L.P.Kadanoff, Phys.Rev. B **28**, 3110 (1983)
- [173] C.K.Harris and R.B.Stinchcombe, Phys. Rev. Lett. **50**, 1399 (1983)
- [174] A.C.Maggs and R.B.Stinchcombe, J. Phys. A **19**, 2637 (1986);
R.B.Stinchcombe in: *Order and Chaos in Nonlinear Physical Systems*, eds.: S.Lundquist et al. (Plenum, New York, 1988)

- [175] P.Reichert and R.Schilling, *Phys.Rev. B* **32**, 5731 (1985)
- [176] M.Kohmoto, L.P.Kadanoff and C.Tang, *Phys. Rev. Lett.* **50**, 1870 (1983)
- [177] S.Ostlund et al., *Phys. Rev. Lett.* **50**, 1873 (1983)
- [178] M.Kohmoto and Y.Oono, *Phys. Lett.* **102 A**, 145 (1984)
- [179] J.P.Lu, T.Odagaki and J.L.Birman, *Phys.Rev. B* **33**, 4809 (1986);
 J.Kollár and A.Sütő, *Phys. Lett.* **117 A**, 203 (1986);
 M.Kohmoto and J.R.Banavar, *Phys.Rev. B* **34**, 563 (1986);
 M.Kohmoto, B.Sutherland and C.Tang, *Phys.Rev. B* **35**, 1020 (1987);
 J.A.Ashraff and R.B.Stinchcombe, *Phys.Rev. B* **39**, 2670 (1989);
 M.Kolár and M.K.Ali, *Phys.Rev. A* **39**, 6538 (1989)
- [180] P.Ruján, *Physica* **91 A**, 549 (1978)
- [181] G.Györgyi and P.Ruján, *J. Phys. C* **17**, 4207 (1984)
- [182] P.Szépfolusy and U.Behn, *Z. Phys. B* **65**, 337 (1987)
- [183] S.N.Evangelou, *J. Phys. C* **20**, L511 (1987)
- [184] J.Bene and P.Szépfolusy, *Phys.Rev. A* **37**, 1703 (1988)
- [185] T.Tanaka, H.Fujisaka and M.Inoue, *Phys.Rev. A* **39**, 3170 (1989)
- [186] T.Nattermann and P.Ruján, *Intern.J.Mod.Phys.* **11**, 1597 (1988)
- [187] G.Györgyi and P.Ruján, to be published
- [188] C.C. Rankin and W.H. Miller, *J. Chem. Phys.* **55**, 3150 (1971);
 L.Gottdiener, *Mol.Phys.* **29**, 1585 (1979);
 D.W. Noid, S.K. Gray and S.A. Rice, *J. Chem. Phys.* **84**, 2649 (1986);
 M.Berblinger and C.Schlier, *Chem.Phys.Lett.* **145**, 299 (1988)
- [189] J.M. Petit and M. Hénon, *Icarus* **66**, 536 (1986);
 M.Hénon, *La Recherche* **20**, 491 (1989)
- [190] H.Aref, *Ann.Rev.Fluid.Mech.* **15** 345 (1983)
 S.V.Manakov and L.N.Schur, *Soc.Phys.JETP*, **37**, 54 (1983);
 B. Eckhardt, *Europhys. Lett.* **5**, 107 (1988);
 B. Eckhardt and H. Aref, *Phil. Trans. Roy. Soc. A* **326**, 655 (1988)
- [191] C. Jung, *J. Phys. A* **19**, 1345 (1986)
- [192] B. Eckhardt and C. Jung, *J. Phys. A* **19**, L829 (1986)
- [193] C. Jung and H.J. Scholz, *J. Phys. A* **20**, 3607 (1987); *J. Phys. A* **21**, 2301 (1988)
- [194] B. Eckhardt, *J. Phys. A* **20**, 5971 (1987)

- [195] Blümel and U. Smilansky, *Phys. Rev. Lett.* **60**, 477 (1988)
- [196] B. Eckhardt, *Physica D* **33**, 89 (1988)
- [197] M. Hénon, *Physica D* **33**, 132 (1988)
- [198] C.Jung, in *Finite Dimensional Integrable Nonlinear Dynamical Systems*, eds.: P.G.L.Leach and W.H.Steeb (World Scientific, Singapore, 1988)
- [199] B.Mirbach and H.J.Korsch, *Nonlinearity* **2**, 327 (1989)
- [200] G. Troll and U. Smilansky, *Physica D* **35**, 34 (1989)
- [201] P. Gaspard and S.A. Rice, *J. Chem. Phys.* **90**, 2225 (1989)
- [202] C.Jung and S.Pott, *J. Phys. A* **22**, 2925 (1989); C.Jung, Habilitation Thesis, Bremen, 1989 (in German)
- [203] S.Bleher, E.Ott and C.Grebogi, *Phys. Rev. Lett.* **63**, 919 (1989); S.Bleher, C.Grebogi and E.Ott, *Bifurcation to chaotic scattering*, preprint, 1989
- [204] Z.Kovács and T.Tél, *Thermodynamics of irregular scattering*, preprint, 1989
- [205] C.Jung and P.Richter, *Classical chaotic scattering - periodic orbits, symmetries, multifractal invariant sets*, preprint, 1989
- [206] Q.Chen, M.Ding and E.Ott, *Chaotic scattering in several dimensions*, preprint, 1989
- [207] U.Smilansky, in *Chaos and Quantum Physics*, eds.: M.-J.Giannoni et al, (Elsevier, New York, 1990), to appear
- [208] P. Gaspard and S.A. Rice, *J. Chem. Phys.* **90**, 2242, 2255 (1989)
- [209] R.Blümel and U.Smilansky, *Physica D* **36**, 111 (1989)
- [210] P.Cvitanović and B.Eckhardt, *Phys. Rev. Lett.* **63**, 823 (1989)
- [211] R.Blümel and U.Smilansky, *Phys. Rev. Lett.* **64**, 241 (1990)
- [212] C.Jung, *Fractal properties in the semiclassical scattering crosssection of a classically chaotic system*, preprint, 1989;
C.Jung and S.Pott, *Semiclassical crosssection for a classically chaotic scattering system*, preprint, 1990
- [213] W.H.Press et al., *Numerical Recipes* (Cambridge U. Press, Cambridge, 1986)
- [214] N.Packard et al., *Phys. Rev. Lett.* **45**, 712 (1980);
F.Takens, *Lect. Notes in Math.* **898**, 366 (1981)
- [215] G.King, *Chaotic dynamics on a catastrophe manifold*, preprint, 1987

- [216] H.O.Peitgen and P.Richter, *The Beauty of Fractals* (Springer, Berlin, 1986);
O.E. Rössler, C. Kahlert, J. Parisi, J. Peinke and B. Rohricht, *Z. Naturforsch.* **41a**,
819 (1986);
C.Kahlert and O.E.Rössler, *Z.Naturforsch.* **42a**, 324 (1986);
D.Saupe, *Physica D* **28**, 358 (1987)
- [217] L.P.Kadanoff, *Physica Scripta.* **T19**, 19 (1987)
- [218] S.Vaianti, *Il Nouvo Cim.* **99**, 77 (1987);
G.Servizi, G.Turchetti and S.Vaianti, *J. Phys. A* **21**, L639 (1988);
M.Nauenberg and H.J.Schellnhuber, *Phys. Rev. Lett.* **62**, 1807 (1989);
B.Hu and B.Lin, *Phys.Rev. A* **39**, 4789 (1989)
- [219] T.Bohr et al., *Europhys.Lett.* **6**, 445 (1988);
I.Procaccia and R.Zeitak, *Phys. Rev. Lett.* **50**, 2511 (1988)
- [220] J.E.Bayfield and P.M.Koch, *Phys. Rev. Lett.* **33**, 258 (1974);
R.V.Jensen, *Phys. Rev. Lett.* **49**, 1365 (1982)
- [221] B.A.Huberman and W.F.Wolff, *Phys.Rev. A* **32**, 3768 (1985);
W.F.Wolff and B.A.Huberman, *Z. Phys. B* **63**, 397 (1986)
- [222] A.Fulinski and A.Kleczkowski, *Physica Scripta* **35**, 119, (1987)
- [223] P.Cvitanović, in *Group Theoretical Methods in Physics*, ed.: R.Gilmore (World
Scientific, Singapore, 1987)
- [224] D.Katzen and I.Procaccia, *Phys. Rev. Lett.* **58**, 169 (1987)
- [225] P.Szépfolusy, T.Tél, A.Csordás and Z.Kovács, *Phys.Rev. A* **36**, 3525 (1987)
- [226] M.H.Jensen and T.Bohr, *Phys.Rev. A* **36**, 4904 (1987)
- [227] A.Csordás and P.Szépfolusy, *Phys.Rev. A* **39**, 4767 (1989); *Phys.Rev. A* **40**, 2221
(1989)
- [228] T.Morita et al., *Prog. Theor. Phys.* **79**, 296 (1988);
T.Horita et al., *Prog. Theor. Phys.* **80**, 793 (1988);
H.Hata et al., *Prog. Theor. Phys.* **80**, 809, (1988);
T.Yoshida et al., *Prog. Theor. Phys.* **82**, 879 (1989)
- [229] E.Ott, C.Grebogi and J.A.Yorke *J. Phys. A* **21**, L763 (1988)
- [230] Z.Kaufmann and P.Szépfolusy, *Phys.Rev. A* **40**, 2615 (1989)
- [231] J.Bene, P.Szépfolusy and A.Fülöp, *Phys.Rev. A* **40**, 6719 (1989)
- [232] T.Bohr, M.Jensen, A.W.Pedersen and D.Rand, in *Nonlinear Evolution of Spatio-
Temporal Structures*, eds.: F.Busse, L.Kramer (Reidel, New York, 1990)